Catena 260 (2025) 109433

Contents lists available at ScienceDirect

Catena

journal homepage: www.elsevier.com/locate/catena

Evaluating the impact of different agropastoral practices on wind erosion in western Sahel

Paul-Alain Raynal [a,*], Jean-Louis Rajot [a,b,d], Beatrice Marticorena [b], Abdourahmane Tall [c], Baptiste Lemaire [a], Jean-Alain Civil [a], Diouma Cor Fall [c], Gualbert Seraphin Dorego [c], Ibrahima Sarr [c], Issa Faye [c], Ambre Emmendoerffer [b], Henri Guillaume [b], Christel Bouet [a,b], François Affholder [e], Babacar Faye [f], Yélognissè Agbohessou [e,g], Caroline Pierre [a]

[a] Sorbonne Université, Université Paris Cité, Univ Paris Est Creteil, CNRS, IRD, INRAE, Institut d'écologie et des sciences de l'environnement de Paris, IEES, F-75005 Paris, France
[b] Univ Paris Est Creteil and Université Paris Cité, CNRS, LISA, F-94010 Créteil, France
[c] ISRA - Centre National de la Recherche Agronomique (CNRA), Bambey, Senegal
[d] LMI IESOL, Centre IRD-ISRA de Bel Air, BP1386, CP18524 Dakar, Senegal
[e] AIDA, Univ Montpellier, CIRAD, Montpellier, France
[f] Université du Sine Saloum El Hadj Ibrahima Niass (USSEIN), Kaolack, Senegal
[g] CIRAD, UPR AIDA, Montpellier F-34398, France

ARTICLE INFO

Dataset link: Evaluating the impact of different agropastoral practices on wind erosion in western Sahel (Original data)

Keywords:
Wind Erosion
Sahel
Senegal
Land Uses
Agricultural practices

ABSTRACT

In the Sahel, nutrient-poor sandy soils are vulnerable to wind-driven erosion and can be further degraded if left unprotected. As more than 60 % of the Sahelian population depends on rainfed agriculture, land degradation is a primary concern. In the last 60 years, climatic and socio-economic factors have thoroughly modified the Sahelian cropping systems. Understanding the interaction between land uses, agropastoral practices and wind erosion is crucial.

This study aims to estimate the effect of the main types of land uses and management that occurred in the Senegalese groundnut basin in the last decades on potential wind erosion of soil at the field scale. *In-situ* measurements of meteorological data, vegetation and horizontal fluxes of aeolian sediments were monitored on the land uses of a typical Sahelian landscape (groundnut plot, four fallows, four millet plots), each with contrasting and representative land managements, creating an unprecedented dataset in this region. We developed a modeling approach combining vegetation models with a horizontal flux model, calibrated on the gathered data. This modeling approach was able to reproduce existing measurements and is intended eventually to upscale fluxes of aeolian sediment at the landscape to regional scales.

Measurements of horizontal fluxes of aeolian sediments ranged from 538.7 $kg.m^{-1}.year^{-1}$ on bare soil to almost no flux on fallows. Simulations accurately represent the dynamics and order of magnitudes of erosive events despite having a strong sensibility to the aerodynamic roughness length of the soil surface. The comprehensive simulation of the impact of groundnut, millet (with and without residues) and fallows on potential wind erosion highlights the impact of dry vegetation cover, especially weeds, after the rainy season.

1. Introduction

In the last 60 years, cropping systems in the Sahel were altered due to climatic and socio-economic factors (Lericollais, 1970; Badiane et al., 2000; Brandt et al., 2014). This led in some places to a large expansion of croplands to the detriment of natural land covers, in an region where more than 60 % of the population lives in rural areas and depends on rainfed agriculture for subsistence and income (OECD, Sahel and West Africa Club, 2014). For instance, in Burkina Faso, land used for rainfed agriculture grew from 15 percent of the country surface in 1975 to 39 percent in 2013 (Tappan et al., 2016). In Senegal, total agricultural land area remained stable in that period due to the expansion of croplands in

* Corresponding author at: Institute of Ecology and Environmental Sciences (iEES-Paris), Paris, France.
E-mail address: paul-alain.raynal@ird.fr (P.-A. Raynal).

https://doi.org/10.1016/j.catena.2025.109433
Received 17 March 2025; Received in revised form 16 July 2025; Accepted 4 September 2025
Available online 18 September 2025

central Senegal while northwestern croplands were abandoned (Pires, 2012; Tappan et al., 2016). The growing pressure on agricultural land has been at the expense of fallowing areas, used to regenerate soil nutrients (Freeman, 1982; Buldgen et al., 1993), which drastically decreased since 1960 (Masse et al., 2018).

These changes of land uses and practices have a direct effect on land degradation through loss of natural areas (Nzabarinda et al., 2021) and the lack of nutrient restoration through fallowing (Tschakert, 2004). On top of affecting soil fertility or biodiversity (Zabel et al., 2019), intensification and extension of croplands are also thought to play a role in increasing the susceptibility of soil to wind erosion (Lee et al., 2012; Chi et al., 2019), especially in drought prone environments (Leys et al., 2001; Wiggs and Holmes, 2011; Lee and Gill, 2015). Indeed, wind erosion occurs in area with unprotected, dry and loose soils, and semi-arid agropastoral lands are especially vulnerable to wind erosion. It causes fine and nutrients-enriched particles from the topsoil to be transported to their immediate surrounding (creeping, saltation) or into the atmosphere (suspension) (Sterk, 2003). Studies have shown that the replacement of fallows by cropland increased wind erosion (Rajot, 2001; Pierre et al., 2018), especially if no crop residues are left on field after the harvest (Sterk, 2003; Abdourhamane Touré et al., 2011). The resulting movement of matter and nutrients can generate local or regional land degradation, especially when occurring in already nutrient poor soils such as in arid and semi-arid areas (Mainguet and Chemin, 1991; Visser and Sterk, 2007; Doso Jnr, 2014).

Estimates have been made of soil displacement caused by saltation, especially in central and eastern Sahel, ranging from net positive values in fallows due to dust deposition (Rajot, 2001) to net losses of 25 to 50 t. $ha^{-1}.y^{-1}$ in southwestern Niger fields (Bielders et al., 2000, 2001). Sterk et al. (1996) quantified nutrient losses by wind in a millet field in southwestern Niger. The content of carbon and nutrients (potassium, nitrogen and phosphorus) lost in the displaced sediments was near the necessary nutrient uptake of a millet field for a year, as a loss of 57.1 kg. ha^{-1} K, 79.6 kg.ha^{-1}C, 18.3 kg.ha^{-1}N and 6.1 kg.ha^{-1}P was estimated. Wind erosion has been observed in drylands around the globe – in South Africa, China, the USA, or Australia –, highlighting its role in soil degradation (Lyles, 1975; Gillette and Hanson, 1989; Mctainsh et al., 1990; Sterk et al., 2001; Nordstrom and Hotta, 2004; Li et al., 2007; Wiggs and Holmes, 2011; Guo et al., 2014, Webb et al., 2017).

On top of being detrimental to soil productivity, the mineral dust generated by these events can then have great impact on human health, air pollution and local or global climate (Middleton, 2017; Kok et al., 2023). While this is an important concern for population depending on rainfed agriculture (Bielders et al., 2004), few studies are dedicated to estimate and compare the effect of the main agropastoral practices (e.g., type of crops, fallowing, residue collection, grazing) on wind erosion in the Sahel (Sterk et al., 1996; Rajot, 2001; Bielders et al., 2001; 2002; Abdourhamane Touré et al., 2011, 2019).

To assess horizontal flux production caused by change in agropastoral practices at larger scales – both temporal and spatial –, it is necessary to rely on modeling wind erosion, especially in relation to land use and management. While several studies proposed models for wind erosion on cropland, often originally designed for US croplands (Woodruff and Siddoway, 1965; Hagen, 1991), modeling the impact of land use and management on wind erosion has only been attempted in the Sahel in a small number of studies (Visser et al., 2005; Pierre et al., 2014a; 2015; 2018), especially for pastoral areas and millet fields.

Thus, the objective of this study is first to estimate through *in situ* measurements the effect of different representative agropastoral practices on flux generation at a plot level on the typical sandy soils of Sahelian Senegal. Secondly, this study aims to develop a modeling approach capable of reproducing the horizontal flux generation for land uses of typical Sahelian landscapes. We present here a complete and unique dataset of meteorological conditions, vegetation characteristics and aeolian sediment fluxes for past (1950–1960) and modern agropastoral practices in western Sahel (Senegalese groundnut basin). This dataset is used for the development and calibration of our modeling approach, combining vegetation models designed for the Sahelian crops and conditions, and a horizontal flux model, allowing the accurate estimation of aeolian sediment fluxes at the plot level for several land uses and management within the same framework. These characteristics (Sahelian representativeness, bottom-up approach), as well as a dataset encompassing a wide array of land uses and practices, represent an advance in modelling wind erosion in the Sahel, which could contribute to a better understanding of the anthropic role in soil degradation and aeolian sediment flux generation in a critical area.

2. Material and methods

2.1. Study sites

The Sahel is defined by the north–south gradient of annual precipitation ranging from 200 to 600 mm (Lebel and Ali, 2009). The rainy season, which lasts from July to October, is critical for vegetation development and determines the state of the soil cover for the following dry season, when green vegetation turns into straw and litter. Sahelian soils usually have a sandy-loam texture, with low organic matter content and poor fertility (Sterk, 2003). During the long dry season, these soils are often unprotected and can be strongly affected by wind erosion (e.g., Bielders et al., 2004). In central Sahel, the start of the monsoon (May-June) is accompanied by strong winds due to mesoscale convective systems (MCS) while the vegetation cover is at its lowest, generating most of the annual wind-driven erosion (Bielders et al, 2004; Bergametti et al., 2020). This is different in the western Sahel where in-situ observations showed that wind erosion occurs from February to June, and is caused by winds just above the erosion threshold (Pierre et al., 2023).

The groundnut basin in Sahelian Senegal (14–16.5° in latitudes, Fig. 1) concentrates most of Senegalese arable land, with a central cereal-leguminous rotation system (millet and groundnut) accompanied by several secondary crops (cowpea, maize) (Garambois et al., 2024, Lericollais et al., 1999). From the Senegal river delta to the south of the groundnut basin, homogenous landscapes of sandy flatlands dominate, with scattered woody vegetation and few degraded forest patches (Pélissier, 1966; Faye & Du, 2021). Soils in the groundnut basin are usually divided into two broad categories –*Dior* and *Deck*- which are respectively considered arenosols and fluvisols under the international soil classification (IUSS Working Group WRB, 2015): *Dior* soils are tropical ferruginous soils with a coarse sand texture and low amounts of organic matter. These soils occupy most of the groundnut basin and make for 70 % of cultivated soils around Bambey (Diallo et al., 2017; Tschakert & Tappan, 2004). *Deck* soils, richer in clay content (5–10 %) and often found in inter-dunal depression and shallows, these soils are often more fertile due to higher organic matter and clay content. They have a better structure and water holding capacity, making them less vulnerable to wind erosion (Zobeck, 1991; Cissokho, 2011). We monitored sites in the groundnut basin as testing grounds for investigating the impact of historical Sahelian agricultural practices and their trajectory at regional scale in the last 60 years on wind erosion. For 4 years, 9 plots were instrumented (1 plot of groundnut for 2 years, 4 fallows for one year, and 4 plots of millet for one year, each plot size being approximately 1 ha). For each, we monitored weather conditions, vegetation growth, and horizontal flux of sediments. In order to allow the comparability between observations made during different years, plots studied during the same year were adjoining (see Appendix A.), ensuring similar weather conditions, while inter annual comparison was made possible by taking into account wind patterns, erosivity and rainfall (Appendix B., Section 3.1.1.).

The groundnut and millet plots are located in Bambey (14°43′16.84″N, 16°29′26.95″W), on the grounds of the Senegalese Institute of Agricultural Research (ISRA/CNRA). The groundnut plot (GN0) was monitored from February 2020 to January 2022. To estimate maximum potential flux over unprotected soil and bare soil properties,

Fig. 1. Left: Satellite image of Senegal. The Groundnut Basin (in yellow) and the Ferlo (in green) compose the Sahelian Senegal. The two study sites are located in the Diourbel region of the groundnut basin (red dots). Satellite Image Credit: European Union, contains modified Copernicus Sentinel data 2025, processed with EO Browser. Right: Drone photography of studied fallows (top) and millet plots (bottom). (Photo Credit: Jean-Louis Rajot).

the field was cleared and plowed in early 2020 (Fig. 2a), leaving a homogenous and smooth surface. Measurements from February 2020 to June 2020 thus depict the response of bare soil to wind erosion. Groundnut was cultivated during the rainy seasons of 2020 (Fig. 2 b, c) and 2021. The millet plots comprise the plot previously used for groundnut completed by three other adjacent plots. Millet (Souna variety) was cultivated on the four plots (1.5 ha) from June 2023 to June 2024. The four millet plots were planned to differ in management in order to reproduce regional and historical practices: M1 was manually seeded and crop residues were left on the field after harvest (Fig. 2e, h), M2 was seeded with the help of animal traction, and crop residues were collected during the harvest (Fig. 2 f, i). M3 and M4 were respectively the same as M1 and M2 but millet was intercropped with cowpea (seeded between millet rows) on both of these plots, and cowpea was fully harvested before the millet harvest (Fig. 1).

The fallows are located 10 km north of Bambey near the village of Ndem (14°48′25.95″N 16°28′9.42″O.). Four adjacent fallows were monitored from July 2022 to June 2023 (Fig. 2 d, g). The four fallows were chosen because they differ in age and cover type: F1 is a new fallow with residues from the previous year's millet crop, F2 is an older fallow (>2 years) covered in part by *Guiera senegalensis*, a typical Sahelian bush, F3 is a new fallow where groundnut and cowpea were cultivated the year before, and F4 is an older fallow with a higher tree density.

All plots were instrumented with 5 two dimensional sonic anemometers at 1.9, 1.5, 1, 0.6, and 0.2 m (WindSonic ™ Gill Instruments Ltd), and temperature sensors (1.6, 1.2, 0.7, 0.4, 0.03 m) mounted on the same mast placed downwind, and on each site a rain gauge (ARG100 Tipping Bucket, 0.2 mm precision, Campbell® Scientific company for GN0, Environmental Measurements Ltd for other plots), a solar radiation sensor (CMP11, Kipp and Zonen), and a saltiphone (Eijkelkamp, Spaan and Van den Abeele, 1991) to measure sand grain impacts and identify erosion events were placed. These data are measured every 10 s and averaged (cumulated) at a 5-minute resolution for wind and solar radiation (for precipitations and saltiphone). To measure wind-blown sediments, 5 masts of 5 MWAC sand traps (Modified Wilson And Cooke, Sterk and Raats, 1996), placed at 5, 10, 20, 40, and 80 cm on each mast, were installed on all plots and were collected every two weeks dried and weighed with 1 mg precision. To ensure the measurement of only the sediments originating from the plots, on fallows 3 masts of 5 MWAC were located downwind while two others were located on the borders to capture ingoing sediment from neighboring plots. On millet and groundnut plots, all 5 MWAC masts were located downwind (ie., southwestern corner). On millet plots, grass strips were grown around each plot to ensure that no outside flux of sediment is entering the plot. Further details on the experimental setups are provided in Appendix A. From the measurements of sediment mass at different heights, horizontal flux was computed by fitting an exponential equation as proposed by Fryrear and Saleh (1993).

On the groundnut plot vegetation was monitored with height, cover (through photographs following the methodology described in Appendix C), and biomass (destructive) measurements during the 2021 rainy season while weed biomass measurements were taken during the dry season. On fallows and millet plots, vegetation was monitored for the whole year. Height measurements and photographs of vegetation cover were done weekly along two diagonal transects for each plot, and biomass classification and destructive weighing for 6 1x1m^2 (0.9*1.8 m^2 on millet plots) random locations across each plot were done monthly (every two weeks during the rainy season for millet plots). The size and frequency of the sampling are described in Appendix C.

During the monitoring of the groundnut plot, 1.2 % of the data was

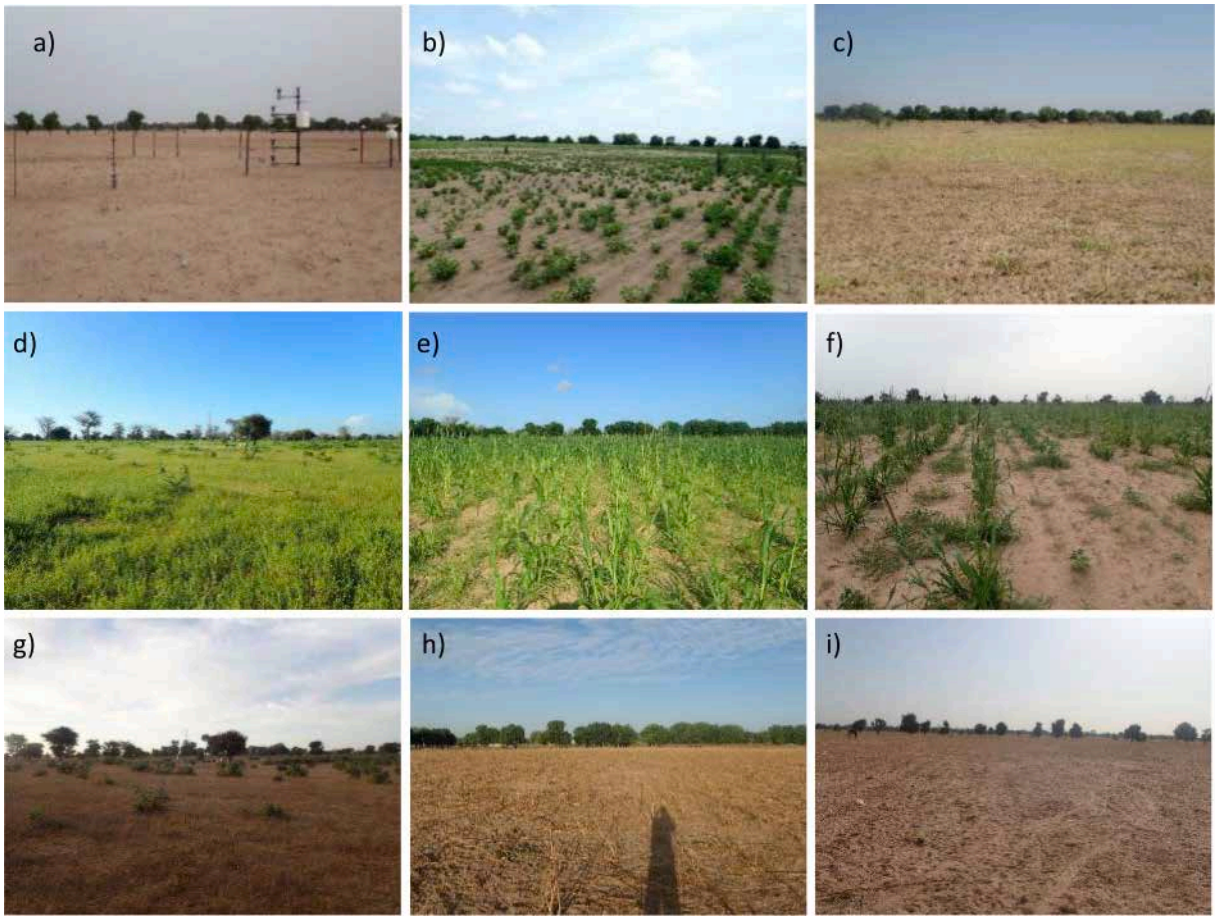

Fig. 2. a-c) Pictures of the groundnut plot in February 2020 when the soil is almost bare, September 2020 during the cropping period and December 2020 after the harvest when weeds occupy a large part of the plot. d-g) Pictures of the fallows from fallow F1 in September 2022 (d) and January 2023 (g). e,f,h,i) Pictures of millet plots M1, M4 in September 2023 (e and f) and January 2023 (h and i) where residues are seen on M1.

lost due to solar-powered battery malfunctioning, mostly between 10 and 25 June 2020, 01 to 12 June 2021, and sporadically between 01 and 21 August 2021. Temperature sensors 1 (lowest sensor), 2 and 5 malfunctioned for longer periods of time leading to the loss of respectively 20 %,10 % and 14 % of their data on different periods.

While the instruments were set up between the 5th and 14th of July 2022 on the fallows, the temperature sensors started operating between the 20th and 21st of July. The higher temperature sensor on the millet plot M4 was defective between the 19th and 27th of July 2023. No other significant missing data is reported during the monitoring. Part of the data of the groundnut plot was presented in Pierre et al. (2023). Complementary meteorological data (wind speed, air temperature, relative humidity, precipitation amount) from the INDAAF (International Network to study Deposition and Atmospheric composition in AFrica) station in Bambey (Marticorena et al., 2021) were used for gap-filling of missing data.

Rainy season start and duration were established using methodology from Sivakumar (1988) in which the onset of the rainy season is defined as the date when at least 20 mm of rain has fallen in 3 consecutive days and no dry spell longer than 7 days happens in the following 30 days, and the end of the rainy season is defined as the date after September 1 after which no rain occurs during a period of 20 days. The mean annual rainfall in Bambey was calculated using data collected by the CNRA of Bambey at a daily timescale.

A grain size distribution analysis of the soil was made for the groundnut plot (which became M4 in 2023). With a sand content close to 95 %, they are typical *Dior* soils, found in most of the area (Table 1). We selected plots with arenosols representative of most of the cultivated soils in Senegal's groundnut basin, both for the millet and groundnut plots (located in exactly the same place as the analyses) and for the fallow land. The measurement sites are located on the same geomorphological unit: flattened quaternary dune tops, with care taken to avoid areas corresponding to former interdune depressions. Hence, the results of the grain size distribution analyses is used as the "reference" soil in this study, meaning these values are used in our models for each simulations.

Table 1
Grain size analysis of the GN0 plot, median and standard of 16 1 m^2 soil surface measurements.

Soil fraction	Coarse sand	Fine sand	Coarse loam	Fine loam	Clay
Median %	34.95	58	2.8	0.15	4.2
Standard deviation	4.97	4.59	0.77	0.45	0.89

2.2. Aerodynamic roughness length estimation method

The aerodynamic surface roughness z_0 is a key parameter to understand and model the generation of horizontal flux, as it determines the wind friction velocity and the threshold friction velocity, i.e. the interaction between the atmosphere and the soil surface.

In neutral atmospheric conditions, the wind profile is logarithmic (Priestley, 1959):

$u(z) = \frac{u_*(t)}{k} \ln\left(\frac{z}{z_0(t)}\right)$ for $z \gg z_0(t)$ with $u_*(t)$ the wind friction velocity.

(1).

It is then possible to estimate, in neutral conditions, the aerodynamic roughness length and the wind friction velocity using only the measured wind profile. In natural conditions, the atmosphere is neutral around sunrise and sunset and is either stable or unstable during the rest of the day, yielding to an estimate of a z_0 time series that relies on a restricted number of values. Using the Similarity Theory from Monin and Obukhov (1954), one describes the wind velocity $u(z)$ in non-neutral conditions as:

$$u(z) = \frac{u_*}{k}\left[ln\left(\frac{z}{z_0}\right) - \Psi m\left(\frac{z}{L}\right) + \Psi m\left(\frac{z_0}{L}\right)\right] \; with \; L = \frac{u_*^2\theta}{kg\theta_*} \quad (2)$$

Where L is the Monin-Obukhov length (m), Ψm is a "stability function", m for momentum and h for temperature, θ the potential temperature (K) and θ_* the temperature scale.

Ψm and Ψh depend on atmospheric conditions, which are determined by the stability parameter z/L, which is lower than 0 in unstable conditions and greater than 0 in stable conditions. Following the iterative fitting procedure developed by Frangi and Richards, 2000 and adapted by Marticorena et al. (2006), the parameters u_*, z_0, θ_* and L can be determined, as well as Ri the Richardson number, which describes the turbulence of the flow and is a function of the stability parameter:

$$Ri = \frac{g}{T}\frac{\partial\theta/\partial z}{\left(\partial u/\partial z\right)^2} \quad (3)$$

Where g is the acceleration of gravity (9.81 $m.s^{-2}$), T the absolute air temperature (K). Low absolute Ri values correspond to conditions close to neutrality.

We adapted the method from Marticorena et al. (2006) in order to produce a z_0 time serie containing only the best reliable z_0 estimates. By defining neutrality thresholds on the Richardson number ($|Ri|<0.005$, $|Ri|<0.02$, $|Ri|<0.2$) and a minimum density of z_0 values for a given time period (set at 30 values in 15 days), we devised a denoising method that respects both the demand for reliable z_0 values (low $|Ri|$ values) and homogenous and dense z_0 time series. z_0 values are only kept in the time serie if they fit the strongest Richardson threshold possible ($|Ri|<0.005$) while also meeting the density criteria. The resulting time series represent an estimation of the aerodynamic roughness length z_0 at a 15 min resolution.

2.3. Modeling approach

To allow for flux estimation in areas without precise in-situ measurements, we combined vegetation development and horizontal flux models calibrated on our dataset (Fig. 3).

Weather data (*in-situ* measurements, climate re-analysis or projections), soil features and agropastoral practices specificities, are used as inputs to a vegetation model. A different vegetation growth model is used for rangeland (Sahelian Transpiration Evaporation and Productivity model – STEP, Mougin et al., 1995) and cropland (Simulateur mulTIdisciplinaire pour les Cultures Standard – STICS, Brisson et al., 2003), both simulating vegetation biomass, height, and cover. These outputs are then used to estimate the aerodynamic roughness length z_0, a key parameter for aeolian horizontal flux modeling. Both the aerodynamic roughness length z_0 and the weather and soil data are inputs to the horizontal flux model (Dust Production Model – DPM, Marticorena and Bergametti, 1995). This approach was used in previous studies in Niger and Mali for a narrower range of conditions and allowed for an accurate simulation of the horizontal flux (Pierre et al., 2014a; 2015).

2.3.1. Vegetation models

The STEP model is designed to simulate the herbaceous vegetation development and degradation in Sahelian soil and meteorological conditions. At a daily timescale, the STEP model describes the soil water budget and vegetation growth based on the site meteorology (rainfall, temperature, humidity, radiation, and wind speed) and characteristics (soil texture and layer depth, grazing pressure, C3/C4 proportions). It has shown a good ability to reproduce observed biomass in previous studies (Tracol et al., 2006; Pierre et al., 2015; Mougin et al., 2019, Agbohessou et al., 2023). The model consists of two submodels describing 1) water budget and 2) vegetation growth and senescence. Soil characteristics such as texture (percentage of clay and sand) are key parameters in the model as they constraint available water for plant development and act as proxy for soil fertility. During the dry season, the dynamics of straws and litter biomass are calculated through the effect of meteorological factors and trampling or ingestion by grazing animals (Delon et al., 2015; Pierre et al., 2015; 2016). Soil productivity is implicitly taken into account in the model through the maximum conversion efficiency of absorbed radiation ε (g/MJ). Finally, the STEP model provides LAI (Leaf Area Index), dry matter biomass of green, straws and litter, and the fraction of soil covered by vegetation at a daily time step.

STICS is a dynamic soil-crop model working at a daily time-step. It is based on several modules simulating processes such as crop growth, yield formation, carbon, water and nitrogen transfer and balances (Brisson et al., 2003). This model was chosen for its ability to simulate different crops and practices, as well as its robustness in different climates: it was well suited to represent crops grown under tropical or semi-arid climate and soil conditions, as demonstrated by its application to sorghum-cowpea intercropping (Traoré et al., 2022), groundnut,

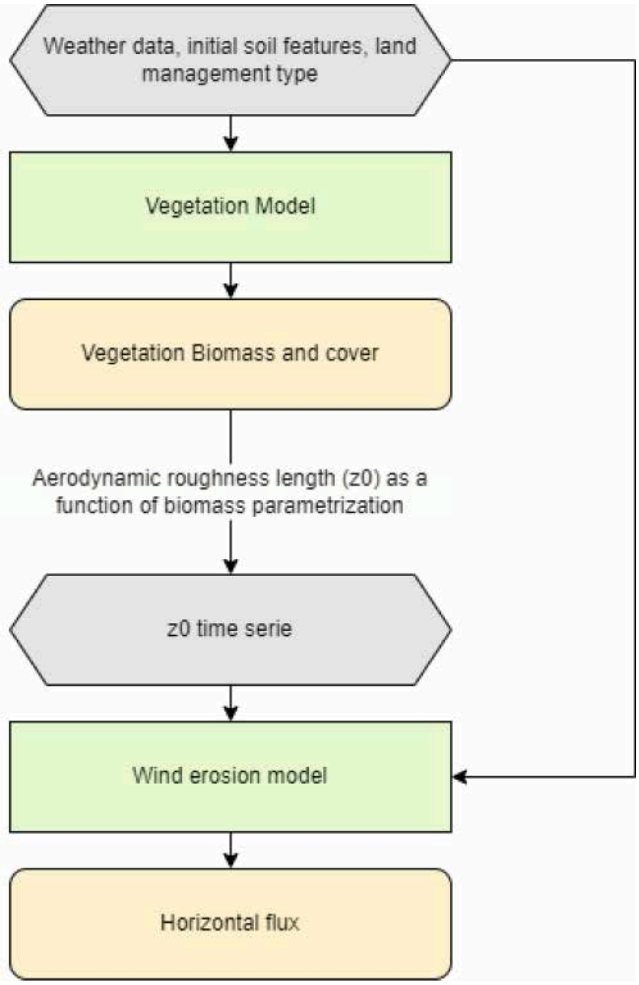

Fig. 3. Diagram of the modeling approach. Gray boxes are inputs, light green boxes are models and orange boxes are model outputs.

millet (Sow et al., 2024) or rice (Ranaivoson et al., 2022).

The model requires inputs similar to STEP for weather and soil conditions. The STICS model has a strong sensibility to soil texture and nutrient content. It also requires field management information such as sowing date, depth and density, fertilization, irrigation and additional practices. Finally, plant parameters, specifying phenological stage durations, leaf growth and harvested organs details are need. In this study, we use a groundnut parametrization presented in Appendix D and millet parametrization from Sow et al. (2024). Because STICS does not handle plant degradation after harvest, an additional module was used for this purpose (Appendix E).

2.3.2. Horizontal flux model

The DPM has been used to estimate horizontal flux of aeolian sediments from the soil at the plot scale in the Sahel in previous studies (Pierre et al., 2014a; 2015, 2018). A brief description of its functioning is given in this sub-section.

Wind erosion occurs when wind friction velocity on the soil exceeds a threshold value. This threshold is a function of the state of the soil surface and of the presence of non-erodible elements such as pebbles or vegetation. The wind drag is partitioned between erodible and non-erodible parts of the soil. This is taken into account through the aerodynamic roughness length z_0 in the DPM model. Once the threshold is exceeded, the wind erosion is a power function of the wind friction velocity.

The wind friction velocity threshold u_{*t} is described as follows:

$$u_{t^*}(z_0, z_{0s}) = \frac{u_{ts^*}}{f_{eff}(z_0, z_{0s})} \quad (4)$$

Where u_{*ts} is the wind friction velocity threshold over bare soil, z_0 (z_{0s}) the aerodynamic roughness length of the surface (bare soil) and f_{eff} the efficient fraction velocity ratio:

$$f_{eff}(z_0, z_{0s}) = 1 - \frac{ln\left(\frac{z_0}{z_{0s}}\right)}{ln\left(\frac{\delta}{z_{0s}}\right)}, \frac{\delta}{z_{0s}} = a^* \frac{X^p}{z_{0s}} \quad (5)$$

δ is the height of the Internal Boundary Layer, and a, X, and p were determined as $a = 0.7$, $X = 0.4$ m, and $p = 0.8$ in previous studies for vegetated surfaces with good agreement with observations (Elliot, 1958; Darmenova et al., 2009; Pierre et al., 2014a). The horizontal flux G is then described as:

if $u_*(t) > u_{t^*}(t)$:

$$G(t) = E^* \frac{\rho_a}{g} * u_{t^*}(t)^3 * \left(1 + \frac{u_{t^*}(t)}{u_*(t)}\right)\left(1 - \left(\frac{u_{t^*}(t)}{u_*(t)}\right)^2\right), \quad (6)$$

else $G(t) = 0$

And the wind friction velocity $u_*(t)$ defined in Eq.1

With z the wind measurement height, E is the erodible fraction ratio (i.e., the soil proportion not covered by obstacles), ρ_a the air density ($1.227*10^{-3}$ kg.m^{-3}). E is taken from vegetation models daily outputs and is adjusted based on weekly photo interpretation as the models tend to underestimate soil cover with a constant bias. $u(z)$ is the wind speed at height z, $k = 0.4$ the Von Karman constant.

Values of z_{0s} and u_{ts^*} are linked to bare soil properties of the cropped plot. We used measurements made between March and May 2020 on GN0 as it was representative of bare soil. z_{0s} was estimated based on the lowest median daily z_0 values of the plot, reaching values between $1.5*10^{-4}$ and $3*10^{-4}$ m (z_0 time series estimation method is described in section 2.2). These values are consistent with other methods of z_{0s} determination based on coarsest grain size diameter (D_{coarse}). Indeed, z_{0s} can be estimated as a function of D_{coarse} as the following:

$z_{0s} = \frac{D_{coarse}}{30}$ (Marticorena and Bergametti, 1995; Laurent et al. 2006) or $z_{0s} = 2\frac{D_{coarse}}{30}$ (Farrell and Sherman, 2006).

Based on the grain size distribution of the plot, 30 % of the soil is made of coarse sand (Table 1), which can range from 0.2 to 2 mm in diameter. This way, z_{0s} range from $6.7*10^{-6}$ m to $1.3*10^{-4}$ m.

u_{ts^*} estimation was made using Abdourhamane Touré et al. (2011) methodology, also used in Pierre et al. (2023). For each month, the u_* value for which the saltiphone had a 50 % chance of activation was computed. The value corresponded to a monthly estimation of u_{t^*}, and u_{ts^*} if the soil is bare. We found u_{ts^*} values ranging from 0.20 m/s to 0.24 m/s, which is consistent with the value of 0.22 m/s for sandy bare soil in Abdourhamane Touré et al. (2011).

For the following, we chose to set z_{0s} between $1.5*10^{-4}$ m and $3*10^{-4}$ m with steps of $0.5*10^{-4}$ m and u_{ts^*} between 0.20 m/s and 0.24 m/s with steps of 0.005 m/s to account for uncertainty in the bare soil surface characteristics.

The horizontal flux G is in kg/m/s, which corresponds to the amount of sediments crossing a 1-meter-wide and infinitely high vertical plane perpendicular to the wind direction during that time period. For a 1 ha field, 1 kg/m equals 0.1 t/ha losses assuming wind is perpendicular to a 100 m side of the field and that no sediment is entering the field.

To account for soil moisture, the simulated horizontal flux was inhibited during rain events and during 12 h following the event, based on previous studies relying on pluriannual observations from Central Sahel (Bergametti et al., 2016).

To compare each land use/management, it is necessary to disentangle the role of wind speed and the role of the soil surface cover. To do so, a ratio G_{DUP} of the total horizontal flux generated during the erosive season G to the associated cumulated Dust Uplift Potential (Marsham et al., 2011; Pierre et al., 2023) has been devised.

$$G_{DUP}(z) = \frac{G}{DUP(z)} * 1000 \quad (7)$$

Where $DUP(z) = u(z)^3\left(1 + \frac{u_t(z)}{u(z)}\right)\left(1 - \frac{u_t(z)^2}{u(z)^2}\right)$ for u > u_t, and 0 otherwise. The DUP was calculated at z = 1.9 m and threshold wind speed $u_t(z)$ was set at 5 m.s^{-1} using the methodology described in Abdourhamane Touré et al. (2019). The DUP is unaffected by vegetation cover, thus G_{DUP} allows for comparison horizontal fluxes, regardless of the year of measure.

3. Results

3.1. Field measurements

3.1.1. Meteorological measurements

Annual rainfall, start and length of rainy season, are shown in Table 2. Compared to the 1999–2019 precipitations, three out of four years are under the mean, 2021 and 2023 being the driest years (almost 60 mm −or 10 %- less than the mean), 2022 being the only study year with rainfall larger than the mean. However, each year of the study is either near (2023) or above the median rainy season duration. Though annual rainfall is the key driver for crop production in the Sahel (Guan et al., 2015), the duration of the rainy season and the onset of the rainy

Table 2
Rainfall summary for all sites and mean for 1999–2019 (Total annual rainfall, rainy season duration and start).

Site (year)	Annual rainfall (mm)	Length of rainy Season (days)	Start of rainy Season
Bare soil (2020)	546	108	July 11
Groundnut (2021)	507.2	99	July 31
Fallows (2022)	649.6	120	July 20
Millet (2023)	506.6	86	August 11
Mean Bambey (1999–2019)	562	87	July 24

season seem to play a large part in crop yield formation (Zhang et al., 2018). With a late onset of the rainy season and low annual rainfall, the groundnut and millet plots were growing in degraded conditions in 2021 and 2023. Millet plots even needed to be resowed due to a dry spell after early rains (Appendix B., figure B.2).

Fig. 4 presents the monthly average wind speed and direction at 1.9 m and precipitation on the groundnut, fallow (F1) and millet (M4) plots. Wind followed three consecutive patterns each year. First, from November to February, the harmattan blew from the north-northeast (330-60°). Then, during spring and summer, winds from the northwest region (330°) increased as their overall speed increased and other winds decreased (65 % of winds coming from the 330° direction occurred between February and June, 95 % of winds over 3.5 m/s coming from the 330° direction occurred between February and June). Wind speed reached a monthly average maximum value in April (3.3 m/s) while most strong winds (>7.5 m/s) during the dry season were recorded in February. Finally, at the start of the summer, wind speed got overall milder during the rainy season (mean dry season: 2.5 m/s, mean rainy season: 1.6 m/s) with the onset of the West African Monsoon as wind began blowing from the southwest (240°). While mean wind speed decreases from the onset of the rainy season until its minimum in October (0.8 m/s), this is also when convective events set the maximum recorded wind speed. All instances of winds over 10 m/s were recorded between June and August, most of the events happening in July. These strong events, despite having the strongest erosive potential, were less frequent than erosive winds from February to April and were less able to generate a flux as they were accompanied by rains and the soil was often covered by vegetation at this point. Recorded winds over fallows were lower than on the fields but the intra-annual dynamic remained the same (Appendix B., Figs. B3, B4).

3.1.2. Vegetation characteristics

Comparison of total sampled biomass for each type of crop/land cover is shown in Fig. 5. Even on cropped plots where multiple weedings occur, the weed biomass was not neglectable as it can reach over 50 g of dry mass/m^2 on millet field. There is an offset between the start of the rainy season and the start of the growing period. Early rains before the start of the rainy season can trigger the growth of weeds which are removed through weedings during the early stage of cropping. Once the crops reach maturity, weeds are not removed as crops are less affected by competition.

Maximum biomass reached on average 140 gDM/m^2 on millet plots, 150 gDM/m^2 on fallows and 60 gDM/m^2 on the groundnut plot. On all plots, the maximum biomass was reached before the end of the rainy season (usually 70 to 80 days after the start of the rainy season). After this peak, post-harvest weeds and millet residues slowly degraded over the course of the dry season reaching biomass ranging from 5 gDM/m^2 for the dry season 2020 weeds to 29 gDM/m^2 for the millet crop residues on M1. Degrading factors include trampling and grazing from animals, as well as biotic (microorganisms) and climatic degradation. Weeds degraded faster than crop residues such as millet stems.

3.1.3. Horizontal flux

Fig. 6 reports the recorded horizontal fluxes. 90 % of the horizontal flux was generated between February and July. Because these measurement were done at different times (from 2020 to 2024), direct comparison of results between years is not possible, and taking into account yearly wind erosivity is necessary. This was done in section 3.3, and dust uplift potential (DUP) on all plots is available in Appendix B. Yet, land uses produced very different order of magnitude of collected horizontal flux, meaning that “first order” comparison remains possible to asses the role of land uses. Difference between land management is not affected by this issue as plots were adjoining.

Winds in the early erosive season (February to April) on GN0 in 2020 were especially strong compared to winds on the same plot in 2021 (Appendix B.). After the 2020 harvest, the plot was left as is and some weeds provided a small cover to the soil as they degraded over the dry season. This combination of factors explains how the horizontal flux was divided by more than 2 between 2020 (538.7 kg/m) and 2021 (194.3 kg/m) (Table 3).

Fallow vegetation is, by definition, not harvested and its degradation is only influenced by weather and grazing livestock. Despite livestock

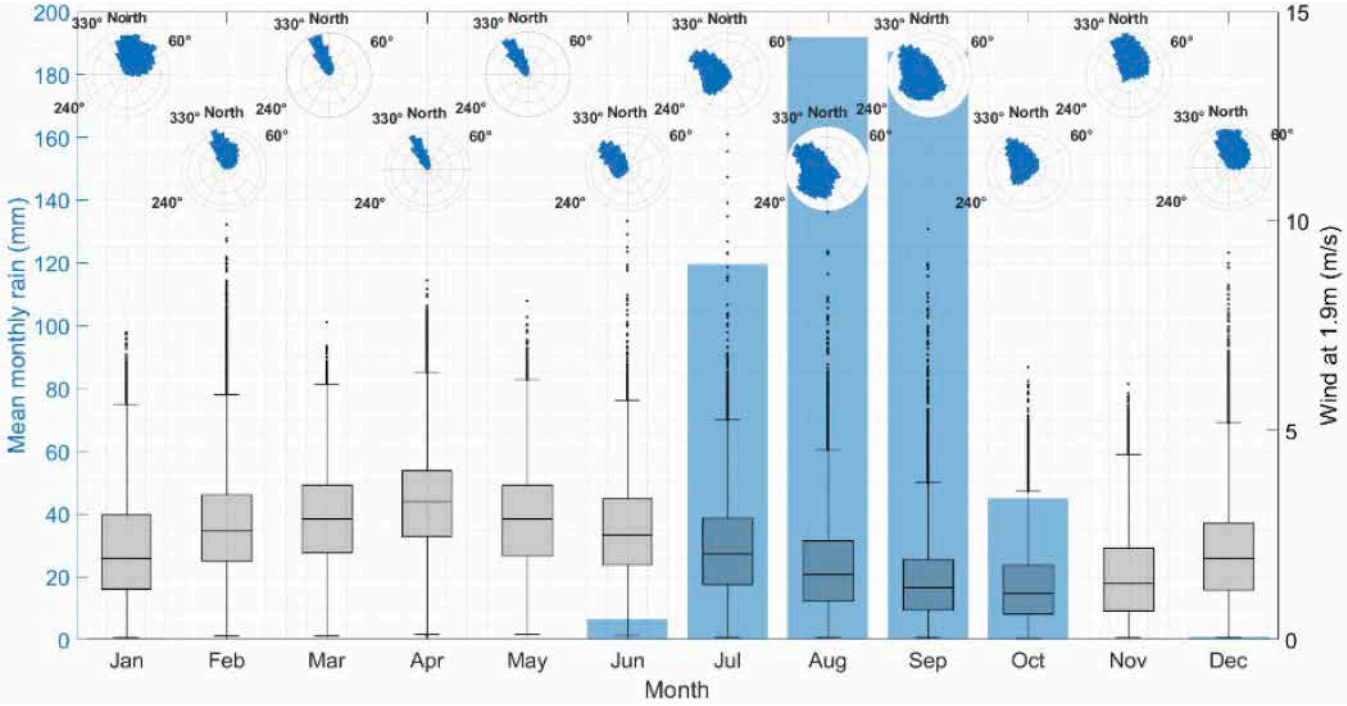

Fig. 4. Monthly weather data from 4 years of records (Feb 2020-Jan 2022, June 2022-July 2024). Mean monthly precipitation are presented in blue bars, monthly aggregated 5 min measurement of winds speeds at 1.9 m are shown in grey boxplots and monthly wind roses on the top.

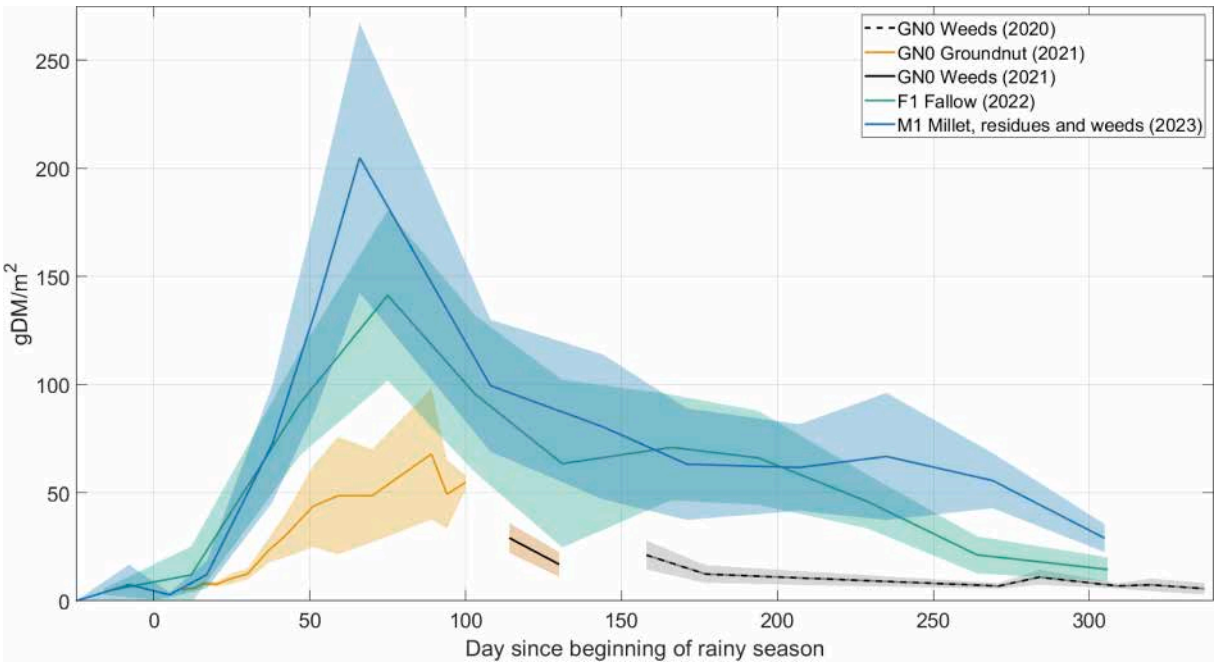

Fig. 5. Measured biomass (in gDM/m^2) on each type of crop and plot.

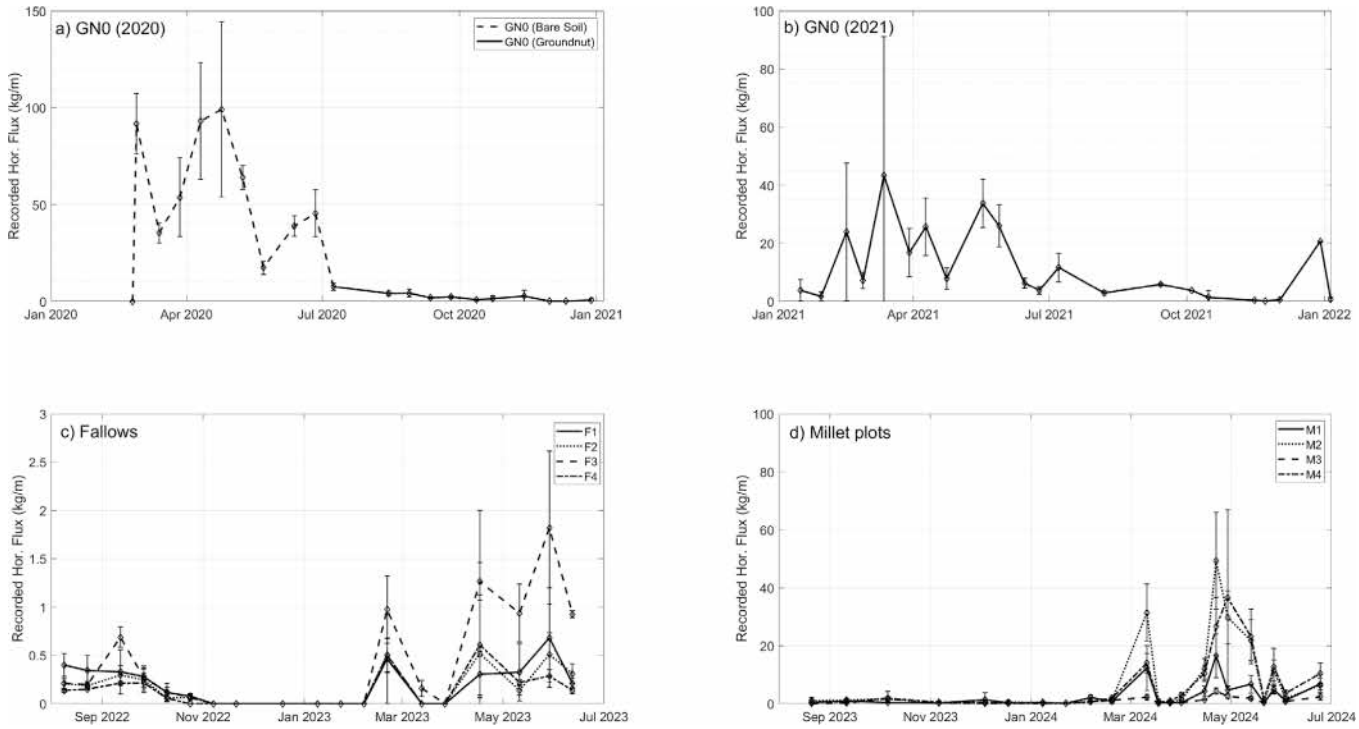

Fig. 6. Recorded horizontal fluxes all plots.

grazing, the soil remained protected most of the year, and the horizontal flux was non-negligible only at the very end of the dry season (sediments collected on May 11, May 29, and June 20) (Fig. 6c). Very low annual amounts of sediments were collected on each fallow (<6.1 kg/m/yr; Tab. 3). However, the collected samples suggest that the various characteristics of fallows played a role in generating horizontal flux. The older fallows (F2: Old fallow with bushes, F4: Old fallow with trees) and the protected young fallow (F1: new fallow with millet residues) were indeed less affected by wind erosion (F4: 1.8 kg/m, F2: 2.0 kg/m, F1: 2.0 kg/m; Tab. 3) than the new unprotected fallow (F3: 6.1 kg/m; Tab. 3).

Measurements of the horizontal flux on millet plots seem to further confirm the role of millet residues on wind erosion mitigation (Abdourhamane Touré et al., 2011; Pierre et al., 2018). Indeed, on millet plots where residues were not collected (M1, M3), horizontal flux was 2 to 7 times lower than on millet plots with residue collection (M2, M4) (Tab. 3). This phenomenon got stronger as weeds degraded on all fields and the only soil protection remaining was prone millet stems during the end of the dry season (Fig. 6d). On millet he yearly horizontal flux ranged from 23.6 to 169.4 kg/m (Tab. 3), the main driver of difference

Table 3
Annual recorded horizontal fluxes on each plot and number of measurements with non-negligible sediment mass (15 days between each sample collection). For fallows and millet measurements are from plot 1 to 4 going from left to right.

Site (year)	Recorded horizontal flux (kg/m, Feb-July)			
Bare soil (2020)	538.70 +/- 62.14			
Groundnut (2021)	194.34 +/- 56.19			
Fallows (2022)	1.98+/- 0.79	1.97 +/- 1.51	6.07 +/- 0.94	1.75 +/- 0.55
Millet (2023)	61.57 +/- 11.69	169.4 +/- 23.33	23.59 +/- 3.06	145.81 +/- 34.49

was the presence of crop residues on the plots.

3.1.4. Aerodynamic roughness length estimation

Using wind profile measurements on each plot, a denoised estimation of aerodynamic roughness length was obtained at a 15 min timescale. To catch the smooth signal of the surface characteristics, the z_0 time series was estimated through daily medians. Using this method, a final z_0 time series derived from observations was defined for each plots, with an associated smoothed $z_0(t)$ time serie (30 days rolling median centered on t) used for horizontal flux simulations (Fig. 7).

On all plots, z_0 values increased during the growing period of the vegetation, ranging from less than a millimeter at the end of June to almost 10 cm in October, at the peak of the rainy season. During the following dry season, the aerodynamic roughness length decreased as the remaining vegetation degraded. Fallows (excepted F4) ware more stable than cropped plots, with z_0 values usually between few millimeters and few centimeters, while groundnut and millet plots can reach much lower z_0 values. z_0 values obtained with this method are further discussed in 4.3.

3.2. Modeling approach

Model calibration was achieved thanks to the field measurement. An in-depth description of the model calibration is presented in Appendix F. The main steps were as such:

- Calibrate the vegetation models using vegetation measurements of the plots. We used modulation of grazing pressure and soil fertility in order to fit the observations. Overall, we were able to reach a strong agreement between the model outputs and the vegetation biomass measurements.
- Parametrization of the aerodynamic roughness length z_0 link with vegetation characteristics. We combined existing relations (Abdourhamane Touré et al., 2011; Pierre et al., 2015, 2018) with observations of wind profiles in order to propose equations linking z_0 with vegetation for each type of land use.
- Creation of the z0 time series using vegetation model outputs for each type of land use and land management.

3.3. Simulated horizontal flux

For horizontal flux simulations, two z_0 time series were used for each plot to validate aerodynamic roughness length simulation against *in-situ* estimations. $z_{0\ est}$ was estimated from wind profile as described in 3.1.4. $z_{0\ sim}$ was derived from biomass simulations and z_0 parametrizations as described in Appendix F.

Horizontal fluxes during erosive season (February – July) are reported in Table 4 for sand traps observations and for simulations. Each simulated flux is the mean of the simulations with all values of u_{*ts} (0.20 – 0.24 m/s) and z_{0s} ($1.5*10^{-4}$ – $3.0*10^{-4}$ m). R^2 and RMSE are calculated by comparing individual sand trap records with cumulated simulated flux between two sand trap observations. For fallows and millet fields, averaged results per land use are also presented to allow for comparison between land uses and practices.

From February to July 2020, the recorded horizontal flux originated from the bare surface and was representative of the response of a bare soil to wind erosion (Fig. 8a). Both $G(z_{0\ est})$ and $G(z_{0\ sim})$ accurately follow the dynamic of the recorded horizontal flux, with a large event at the end of February 2020, and two erosive periods in April and in June 2020. Both simulations for the bare surface overestimates the annual flux ($G(z_{0\ est})$: 653.38 +/- 121.49 kg/m, $G(z_{0\ sim})$: 822.08 +/- 118.25 kg/m, recorded flux: 538.70 +/- 62.14 kg/m) while remaining in or close to the range of the standard deviation. This is caused by an overestimation of some strong erosive events by the model (22 to 27 February 2020) and simulated yet not observed events in late July 2020

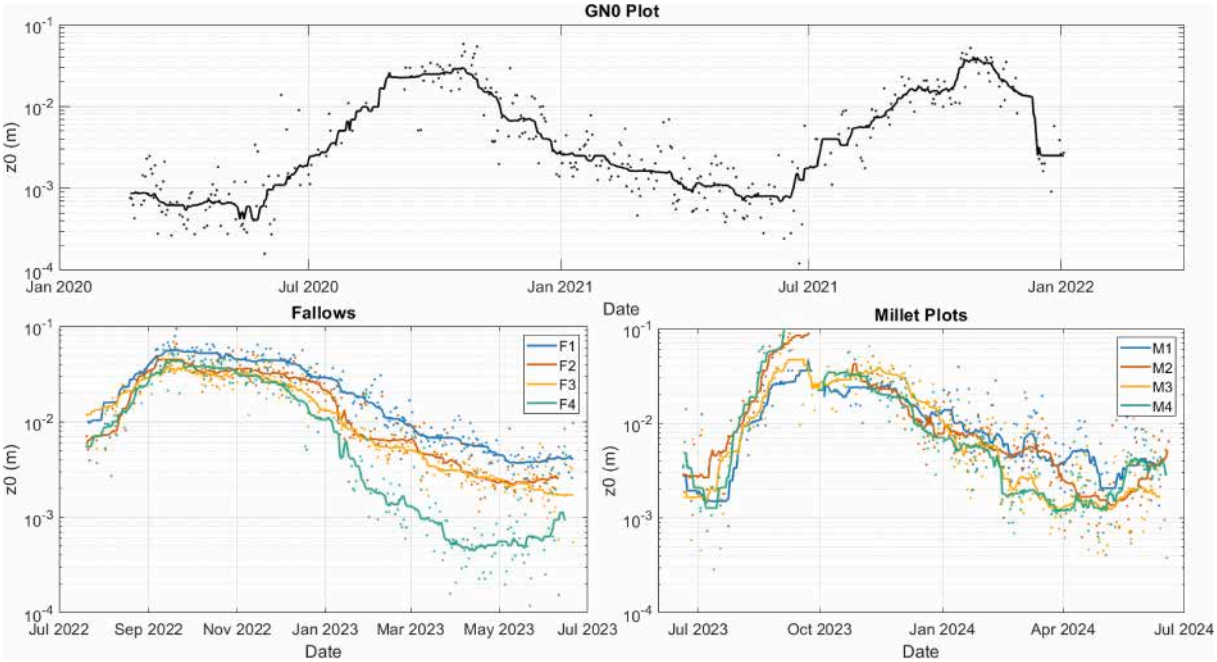

Fig. 7. Observed z_0 time series for all plots. Dots are daily medians, lines are 30 days rolling medians.

Table 4
Summary of observed and simulated fluxes for all plots, standard deviation on simulations is due to variation of u_{ts^*} and z_{0s} values. F, M res and M no res are respectively the mean horizontal flux over the fallows, millet plots with residues and Millet plots without residues.

Name	GN0 (Baresoil)	GN0 (Groundnut)	F1	F2	F3	F4	F	M1	M2	M3	M4	M res	M no res
G(obs)	538.7 +/- 62.14	194.34 +/- 56.19	1.98 +/- 0.79	1.97 +/- 1.51	6.07 +/- 0.94	1.75 +/- 0.55	2.94 +/- 2.08	61.57 +/- 11.69	169.4 +/- 23.33	23.59 +/- 3.06	145.81 +/- 34.49	42.58 +/- 26.85	157.6 +/- 16.67
$G(z_{0\ est})$	653.38 +/- 121.49	256.19 +/- 81.91	0 +/- 1.09	13.3 +/- 30.66	0.35 +/- 3.92	94.95 +/- 48.82	27.15 +/- 45.62	14.46 +/- 24.08	261.73 +/- 90.99	415.36 +/- 116.04	422.72 +/- 111.99	214.91 +/- 283.47	342.23 +/- 113.83
$G(z_{0sim})$	822.08 +/- 118.25	86.92 +/- 34.48	1.83 +/- 2.66	0.24 +/- 0.45	0.45 +/- 0.73	0.02 +/- 0.09	0.63 +/- 0.81	12.78 +/- 13	182.97 +/- 75.93	67.9 +/- 43.14	250.01 +/- 98.35	40.34 +/- 38.97	216.49 +/- 47.41
R^2 (z_{0est}, Obs)	0.71	0.8	0	0.18	0.08	0.42	0.17	0.32	0.91	0.2	0.3	0.26	0.6
R^2 (z_{0sim}, obs)	0.92	0.48	0.32	0.2	0.38	0.01	0.22	0.56	0.92	0.34	0.41	0.45	0.66
RMSE (z_{0est}, obs)	35.83	10.42	0.33	4.51	0.92	17.85	5.9	5.19	16.97	54.55	51.08	29.86	34.02
RMSE (z_{0sim}, obs)	35.44	14.14	0.25	0.29	0.9	0.3	0.43	4.88	7.04	9.36	24.24	7.11	15.63

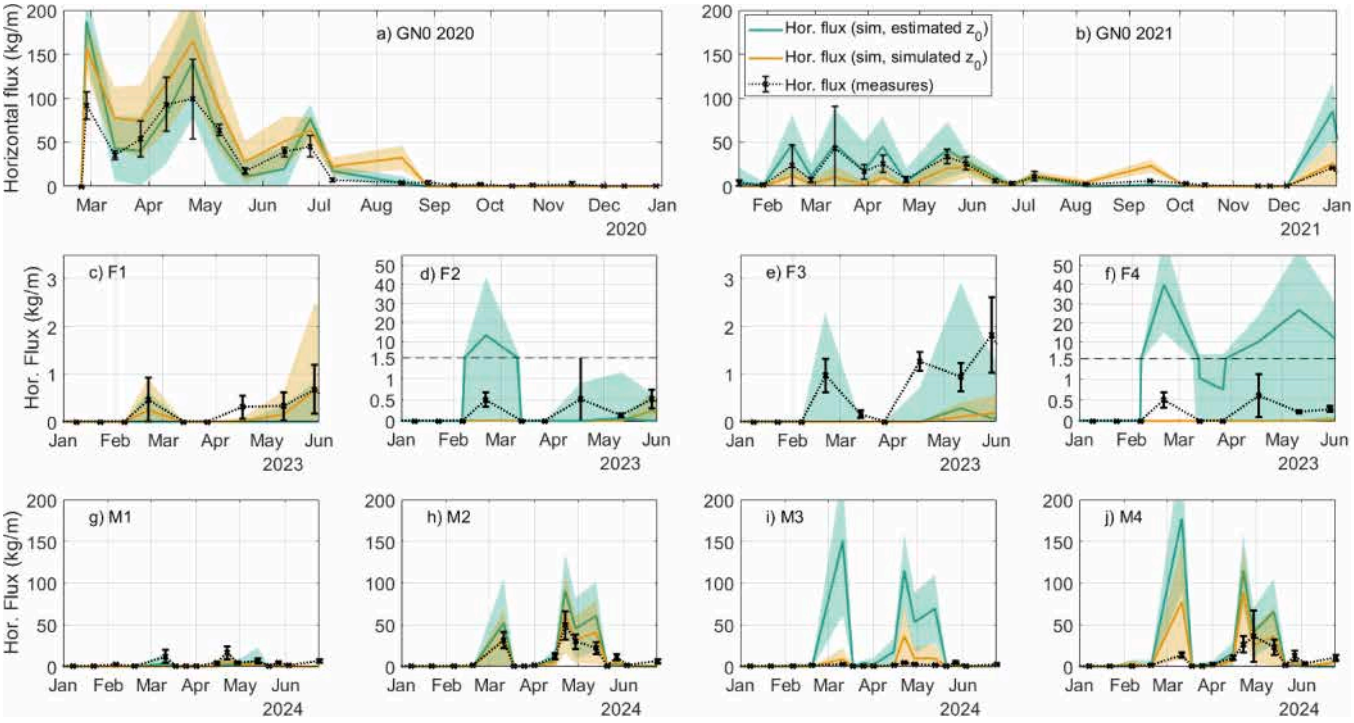

Fig. 8. Simulated and observed horizontal fluxes on all plots. Axis on F2 and F4 have been adapted to display the simulated horizontal flux overestimation for z_{0obs}.

(after seeding) for $z_{0\ sim}$ caused by the underestimation of early vegetation in the STICS model. Yet, the simulation using $z_{0\ sim}$ series performs slightly better in terms of R^2 and RMSE (Table 4) than the one using $z_{0\ est}$, probably because its smoother dynamics through time is closer to the actual surface characteristics.

In 2021, the plot was representative of the aftermath of one year of groundnut cropping. In accordance with the measured flux, the simulated horizontal flux is lower than in 2020 ($G(z_{0\ est})$: 256.19 +/- 81.91 kg/m, $G(z_{0\ sim})$: 86.92 +/- 34.48 kg/m, recorded flux: 194.34 +/- 56.19 kg/m) in similar proportions ($G(z_{0\ est})$: − 61 % from 2020 to 2021, $G(z_{0\ sim})$: − 90 %, recorded flux: −64 %). The simulation with $z_{0\ obs}$ performs better before May 2021 as the flux generated using $z_{0\ sim}$ is underestimated (Fig. 8b). However, horizontal flux recorded after May 2021 are accurately simulated by both series. Uncertainty on weed biomass and parametrization between February and June 2021 may play a role in the underestimation of the flux by $z_{0\ sim}$. The $z_{0\ sim}$ time-serie provides a similar RMSE as $z_{0\ est}$ despite having a worse R^2 score ($R^2_{est} = 0.8$, $R^2_{sim} = 0.48$). For both year and z_0 series, the model is rarely able to simulate very low amounts of horizontal flux (<5 kg/m) as they may happen between September and November.

On the fallows, very low amount of sediment was recorded (1.75 to 6.07 kg/m, Mean: 2.94 +/- 2.08 kg/m), and horizontal flux is mostly generated after May when weed biomass has largely degraded (Fig. 8c to 8f).

Overall, annual horizontal flux simulations were low ($G(z_{0\ est})$: 0.0 to 94.95 kg/m, Mean: 27.15 +/- 45.62 kg/m, $G(z_{0\ sim})$: 0.2 to 1.83 kg/m,

Mean: 0.63 +/- 0.81 kg/m).

Horizontal flux simulations using $z_{0\ est}$ for fallows led to strong flux overestimation on F2 and F4. On F2, it is mainly caused by a single event on 13 February 2023 when wind speeds were oscillating around the threshold velocity, due to the noisy $z_{0\ est}$ time serie. On F4, the stark decrease of $z_{0\ est}$ values in 2023 due to a change of behavior in recorded wind profiles amplifies the overestimation of horizontal flux. Indeed, the measured wind profiles starts to differ from the other fallows after February 2022, as the difference between wind speed measured at 1.9 m and near the surface reduces, leading to a smaller $z_{0\ est}$. The behavior was consistent on all wind speed sensors for F4, excluding the possibility of a sensor dysfunction. Corridor effect originating from tree position or obstacles was investigated both on field and in measured data but no conclusive explanation was found.

Despite these incidents, accurate simulations are obtained for F1, F2 and F3 after April 2023 with $z_{0\ est}$ (Fig. 8c to 8e).

Horizontal fluxes simulated with $z_{0\ sim}$ were not affected by this issue and were in good agreement with recorded fluxes, albeit slightly underestimated. Fluxes generated with $z_{0\ sim}$ may also underline the differences between fallows as F2 and F4 are the less generative according to both observations and the simulated flux. The fluxes generated by $z_{0\ sim}$ consistently had a lower RMSE than $z_{0\ est}$ (respectively for F1 to F4, estimations and simulations RMSE are: 0.33,4.51,0.92,17.85 and 0.25,0.29,0.9,0.3).

Observed sediment fluxes on millet plots can be distinguished between the plots with and without residues (Fig. 8g to 8j). On plots with residues (M1 and M3), the mean total recorded flux was 42.58 +/- 26.85 kg/m from February to July 2024, while on plots where residues were harvested (M2 and M4), the mean total recorded flux was 157.6 +/- 16.67 kg/m during the same period. The overall flux was mostly generated between the end of February and early March and then from April until June. Each of our simulations accurately represents the temporal dynamic of wind erosion on the millet plots. All simulations successfully model larger horizontal fluxes for plots without residues (mean factor of increase for $z_{0\ est}$: 1.6, mean factor of increase for $z_{0\ sim}$: 5.3, mean factor of increase for recorded fluxes: 3.7).

For millet plots without residues, fluxes are mostly accurately modeled by each simulation (Mean fluxes for plots without residues G($z_{0\ est}$): 342.23 +/- 113.83 kg/m, G($z_{0\ sim}$): 216.49 +/- 47.41 kg/m) though with a large uncertainty depending on z_{0s} and u_{ts^*} values. Horizontal flux simulated with $z_{0\ est}$ tends to be overestimated for both M2 and M4. For horizontal flux generated with $z_{0\ sim}$, erosive events during the February-March period are overestimated.

The February-March erosive event on M4 is strongly overestimated in both simulations. Strong harmattan winds (40°, northeastern winds) were blowing during this event and was coincidental to strong decrease of z_0 value for $z_{0\ obs}$.

For millet plots with residues, simulations are less accurate, either because of flux underestimation for M1 (Recorded: 61.57 +/- 11.69 kg/m, G($z_{0\ est}$): 14.46 +/- 24.08 kg/m, G($z_{0\ sim}$): 12.78+/- 13.0 kg/m) or overestimation for M3 (Recorded: 23.59 +/- 3.06 kg/m, G($z_{0\ est}$): 415.36 +/- 116.04 kg/m, G($z_{0\ sim}$): 67.9 +/- 43.14 kg/m). While for M1, both simulated fluxes remain in the same order of magnitude as the recorded flux, M3 is very strongly overestimated by the $z_{0\ est}$ serie and by $z_{0\ sim}$ in a lesser way.

Overall, our modelling approach is able to accurately simulate the horizontal flux on all types of land uses and managements. Despite simulations with low to no vegetations being generally more accurate (R^2 values are consistently higher for low vegetations simulations – GN0, M no res –), we are able to reproduce both similar order of magnitudes and erosive event in most cases, especially when using the z0 time series originating from vegetation simulations.

Comparison between land uses and managements is available in Table 5. Both observed and simulated fluxes rank land uses and managements G_{DUP} from most "erosive" for a bare surface (2.45–3.73) to least "erosive" for fallows (0.01–0.47). Millet plots without residues left on field have a G_{DUP} close to other residue-less crops such as groundnut, while G_{DUP} for millet plots with residue collections are significantly lower for all simulations. The value of G_{DUP} for $z_{0\ est}$ is overestimated for all cases, due to the difficulty of reliable z0 estimation from wind profiles. This however does not affect the overall ranking of land uses from bare soil to fallows.

Table 5
G_{DUP} comparison for observation and simulations.

Land use / Management:	Baresoil	Groundnut	Millet (without residues)	Millet (with residues)	Fallows
G_{DUP}, sand trap measures	2.45	1.37	0.97	0.26	0.05
G_{DUP}, $z_{0\ est}$	2.97	1.81	2.10	1.32	0.47
G_{DUP}, z_{0sim}	3.73	0.61	1.32	0.24	0.01

4. Discussion

4.1. Effect of land uses and land management on the horizontal flux

We found clear difference in generated horizontal flux for each type of land use. The following land use classification in ascending order of yearly horizontal flux was found: Fallows (2.96 +/- 1.91 kg/m) < Millet (100.09 +/- 68.87 kg/m) < Groundnut (194.34 +/- 56.19 kg/m) < Bare soil (538.70 +/- 62.14 kg/m).

These results are consistent with the literature as we expect cropland to produce more horizontal flux than fallows, as already observed in southwestern Niger (Rajot, 2001; Abdourhamane Touré et al., 2011, 2019). Absolute values of horizontal flux are significantly lower than similar studies conducted in western Niger (209 to 601 kg/m/yr, Rajot, 2001; 269 to 619 kg/m/yr, Abdourhamane Touré et al., 2011) and southeastern Niger (368 to 2902 kg/m/yr, Abdourhamane Touré et al., 2019). This difference in horizontal flux intensity is caused by a difference in wind erosion seasonality, as a large additional part of the flux is generated during the onset of the monsoon in Central and Eastern Sahel with strong MCS winds. While dry season winds are similar in central Sahel and Senegal, MCS winds are less intense over Senegal causing most of the erosion to happen between January and May (Pierre et al., 2023).

Horizontal flux originating from bare soil was measured during the dry season of 2020 and represents the maximum possible aeolian flux on a plot. It is not representative of an actual land use as weeds will cover a part of most cultivated plots during the dry season. However, plots managed to have very little to no vegetation cover during the dry season can be accurately represented by the bare soil, even for multiple year. Indeed, while crusting due to rain is a possibility during the rainy season (Casenave and Valentin, 1992), the crusts are quickly destroyed by human trampling during the harvest and animal trampling in the dry season. The deep sandy soils allow aeolian flux generation without supply limitation, as no crust outcrop was observed, even at the end of the dry season.

For groundnut crops, it is to our knowledge the first time horizontal flux has been monitored and modeled in the Sahel, despite it being a major crop in West Africa (Havinden, 1970). To our knowledge, only two studies focus on the link between groundnut crops and wind erosion outside of the Sahel, in India and South Africa (Santra et al., 2017; Vos et al., 2022).

On fallows, larger amounts of sediment seem to be transported on recent, unprotected (no litter cover from previous crop residues) fallows (F3) compared to recent and protected (millet residues left on the fallow) fallows (F1), older fallows with a heavy presence of bushes (F2) or trees (F3). Because recorded fluxes were very low for all cases, it is challenging to measure the impact of woody vegetation on the horizontal flux. However, it seems that bush phenology allowed the observed z_0 value to stay stable from October until January while it

decreased on other fallows, as *guiera senegalensis* leaves stay green until that period. This also played a role in the vegetation cover of the fallows (not shown). Rangeland and fallow vegetation, especially dry vegetation, has been known to mitigate wind erosion in other semi-arid and wind erosion prone areas such as Australia (Aubault et al., 2015), the USA (Li et al., 2007) or Mongolia (Nandintsetseg and Shinoda, 2015).

Millet plots response to wind erosion is mostly affected by the presence of millet residues, as the horizontal flux increased by a factor of 3.8 in the absence of millet residues. It has been shown that a low cover of residue (around 100 kg.ha^{-1}) is enough to reduce the horizontal flux by a factor of 4 in western Niger, and that a quantity of around 800 kg.ha^{-1} of crop residues after harvest would be needed in order to remain over the 100 kg.ha^{-1} threshold at the end of the dry season (Abdourhamane Touré et al., 2019) which is consistent with what our study finds (Millet residues at the start of dry season range from 400 to 650 kg.ha^{-1}, they reach 170 to 270 kg.ha^{-1} in mid-June 2024, while weeds play a more marginal role, with less than 100 kg.ha^{-1} after February).

Other studies on the effect of removing millet residues showed that residue harvesting led to increases of the horizontal flux ranging from a factor of 1.5 to 4 in horizontal flux in Sahelian context (Sterk and Spaan, 1997; Abdourhamane Touré et al., 2011; Pierre et al., 2018). Soil erodible fraction has also been shown to increase with crop residue removal in the American Great Plains (Woodruff and Siddoway, 1965; Skidmore et al., 1979; Nordstrom and Hotta, 2004; Osborne et al., 2014; Blanco-Canqui and Wortmann, 2017; He et al., 2018) and China (Wang et al., 2002; Jia et al., 2015).

An additional conclusion is that on top of millet residues, weeds play a major role in mitigating soil erosion by increasing the surface aerodynamic roughness length during erosive months. After harvest, for both groundnut or millet, the soil is still covered by a non-negligible amount of weeds that degrade over the dry season. The role of weeds for wind erosion mitigation in-between cropping periods has also been described in Mendez and Buschiazzo (2015) for sunflower and corn crops in Argentina.

Recorded horizontal flux on plots seeded using animal traction and intercropped with cowpea (M3 and M4) was slightly lower than their manually seeded without intercropping counterparts (respectively M1 and M2). Because of their development timing (harvested before the main crop), intercrops do not seem to play a noticeable role on flux generation, though they could play an adverse role to animal drawn tillage which loosens the soil in the early rainy season. Differences in observed horizontal flux appears to be correlated to produced biomass left on the plot during dry season rather than to seeding or cropping practices. In Central Sahel where erosive events take place at the onset of the rainy season, tillage and seeding practices may play a more important role.

Overall, our observation further highlights the role of dry vegetation in between rainy seasons in mitigating wind erosion, making groundnut cropping or millet residue harvesting the practices having the most potential for horizontal flux generation, as they were the closest to the maximum flux generation and it is the presence of dry season weed biomass that distinguishes them from bare soil (Table. 5).

4.2. Modeling approach

For both z_0 time series approach, the simulated horizontal flux correctly reproduced the distinction between each type of land use that was measured.

Differences in-between fallows for simulated horizontal fluxes were mostly caused by differences in simulated vegetation biomass, which allowed the models to accurately reproduce the dynamics of horizontal flux generation. Because the STEP model only reproduces herbaceous vegetation, woody vegetation geometry (trees, shrubs) did not have a direct effect on simulated flux generation. As measured and simulated fluxes were close to none (less than 6 kg/m between February and July), relatively high uncertainty remains on the exact result.

For millet plots, the combination of STICS with a degradation module and STEP led to a satisfying simulation of vegetation dynamic on all plots. Maximum simulated z_0 for all millet plots remain under 0.1 m and over 10^{-4}m, which is consistent with the literature (Bielders et al., 2004; Abdourhamane Touré et al., 2011). The absence of residues on plots increased the horizontal flux by a factor of 1.5 to 4.5 depending on the simulation.

To our knowledge, it is the first time weeds developing during the rainy season and left on field during the dry season are modeled alongside the crops. We found that modelling this herbaceous cover is necessary in order to reproduce accurately the soil roughness and associated horizontal flux, which would otherwise be overestimated.

4.3. Remaining limitations

Some sources of plant stresses in STICS can be underestimated, which may be the case for water stress, as soil water has been overestimated in other STICS simulations studies in semi-arid areas (Sow et al., 2024). Some other sources of stress such as phosphorus or anoxia, as well as weeds, pests and diseases are not yet simulated in STICS and may lead to biomass overestimation which was the case for groundnut simulation and in a lesser way for millet plots. The overestimation of groundnut yields was further exacerbated by the crop failure experienced on GN0 in 2021 (Groundnut yield on GN0 in 2021: 0.06 +/- 0.01 t/ha while reported groundnut yields in the peanut basin ranged from 0.4 to 1.5 t/ha, Malou et al., 2021; Sambou et al, 2022). For millet crops simulation, the early development of the plant was poorly reproduced. These parametrizations need refinement in order to be used for horizontal flux simulations in areas where erosion can happen coincidentally to the cropping season, such as central Sahel.

Another uncertainty remains in the estimated z_0 time series derived from wind profile measures. While z_0 values and dynamic is consistent with what is known of the plot surface for most cases, outliers such as F2, F4 or M3 exhibit behavior that do not match with other observations (biomass left on field, horizontal flux measurements).

It is not yet clear what affects the wind speed profiles, though wind direction and obstacles may play a role. Even when z_0 time series accurately reproduce the evolution of the plot surface, they remain noisy and can lead to noticeable flux overestimation.

5. Conclusion

This study proposes a comprehensive dataset of horizontal flux generation associated with each type of main land use and practices in the Sahelian area of the groundnut basin of Senegal and a modelling approach capable of accurately reproducing these land uses and managements, as well as their effect of horizontal flux generation.

The presence of dry vegetation on the plot surface in between rainy seasons is the main way to decrease wind erosion, Therefore, according to our observations, land uses and management that removes most of the plant biomass (groundnut cultivation, millet residue harvesting) after harvest is the most erosive, while leaving crop residues or fallowing almost completely mitigates aeolian flux generation. These observations were reproduced using our modelling approach, with differences in land use and management implemented in a vegetation model and the resulting plant biomass determining surface roughness, a key element in estimating horizontal flux generation. To our knowledge, this modelling framework is the first one allowing for such a comprehensive representation of Sahelian agropastoral practices in regards to wind erosion at this scale. We also present the first study measuring and modeling wind erosion on groundnut crops in the Sahel, despite it being a key West African crop.

Another key result in our study is the role played by weeds in wind erosion mitigation, reducing annual horizontal flux by a factor of 4 to 5 during the dry season for residue-less crops such as groundnut or millet

after residue harvesting. It is thus necessary to model both crops and developing weeds in future studies in order to have an accurate representation of the soil cover and resulting horizontal flux.

With this modelling framework, next steps will consist in broadening the scale of our study. First temporally, by recreating time series of the impact of different agropastoral pathways of the Senegalese groundnut basin on flux generation during the last 60 years and in the future. Then spatially, by describing the horizontal flux generation at the landscape, regional or national scale. Indeed, despite differences in wind seasonality, our study area shows similarity with other Sahelian sites in Niger (Bielders et al., 2000; Rajot et al., 2003; Abdourhamane Touré et al., 2011), Mali (De Rosnay et al., 2009, Pierre et al., 2014b) or northern Burkina Faso (Visser et al., 2005; Leenders et al., 2016) in terms of climate and soil characteristics (sand content higher than 90 %, often close to 95 %, or clay content lower than 5 %) as well as similar agricultural practices. This would make it possible to use our modeling framework right up to the Sahel scale. Then a major main challenge will be the estimation of net soil loss at the regional scale by accounting for the redistribution of aeolian sediment between sources and sink areas.

One remaining open question is that of long term landscape evolution caused by wind erosion. While the presented modelling approach paves the way for future projections, particularly in terms of local soil losses due to wind erosion, soil and nutrient budget at the plot scale are necessary in order to estimate long term displacement of sediment and their budget. Moreover, landscape changes are also dictated by changes in land use and management, probably related to soil fertility changes, but also to policy changes (government subsidies for agricultural mechanizations or input, change in tenure laws) (Garambois et al., 2024; Masse et al., 2018). Estimating future agropastoral management trajectories in the Sahel further requires a fine understanding of its agrarian systems and associated land management (Gangneron et al., 2024). Further research should focus on these trajectories and their impact on soil fertility.

CRediT authorship contribution statement

Paul-Alain Raynal: Writing – review & editing, Writing – original draft, Visualization, Software, Methodology, Formal analysis, Data curation, Conceptualization. **Jean-Louis Rajot:** Writing – review & editing, Supervision, Investigation, Data curation. **Beatrice Marticorena:** Writing – review & editing, Supervision, Methodology. **Abdourahmane Tall:** Investigation, Data curation. **Baptiste Lemaire:** Resources, Data curation. **Jean-Alain Civil:** Software. **Diouma Cor Fall:** Project administration. **Gualbert Seraphin Dorego:** Project administration. **Ibrahima Sarr:** Project administration. **Issa Faye:** Project administration. **Ambre Emmendoerffer:** Software, Data curation. **Henri Guillaume:** Software, Data curation. **Christel Bouet:** Writing – review & editing, Supervision, Data curation. **François Affholder:** Software, Data curation. **Babacar Faye:** Software, Data curation. **Yélognissè Agbohessou:** Data curation, Software. **Caroline Pierre:** Writing – review & editing, Supervision, Project administration, Methodology, Funding acquisition, Conceptualization.

Funding

This work has been supported by the research program LANDWIND (ANR-21-CE01-0024) from the French Agence Nationale de la Recherche.

Declaration of competing interest

The authors declare that they have no known competing financial interests or personal relationships that could have appeared to influence the work reported in this paper.

Acknowledgment

The French National Observatory Service INDAAF is supported by the INSU/CNRS, the IRD (Institut de Recherche pour le Développement), and the Observatoires des Sciences de l'Univers EFLUVE and Observatoire Midi-Pyrénées. The authors would like to thank the French and African PIs and operators for maintaining the INDAAF stations. The authors would also like to thank the Faidherbia-Flux project and platform (https://lped.info/wikiObsSN/?Faidherbia-Flux).

Appendix A. . Instrumental setup

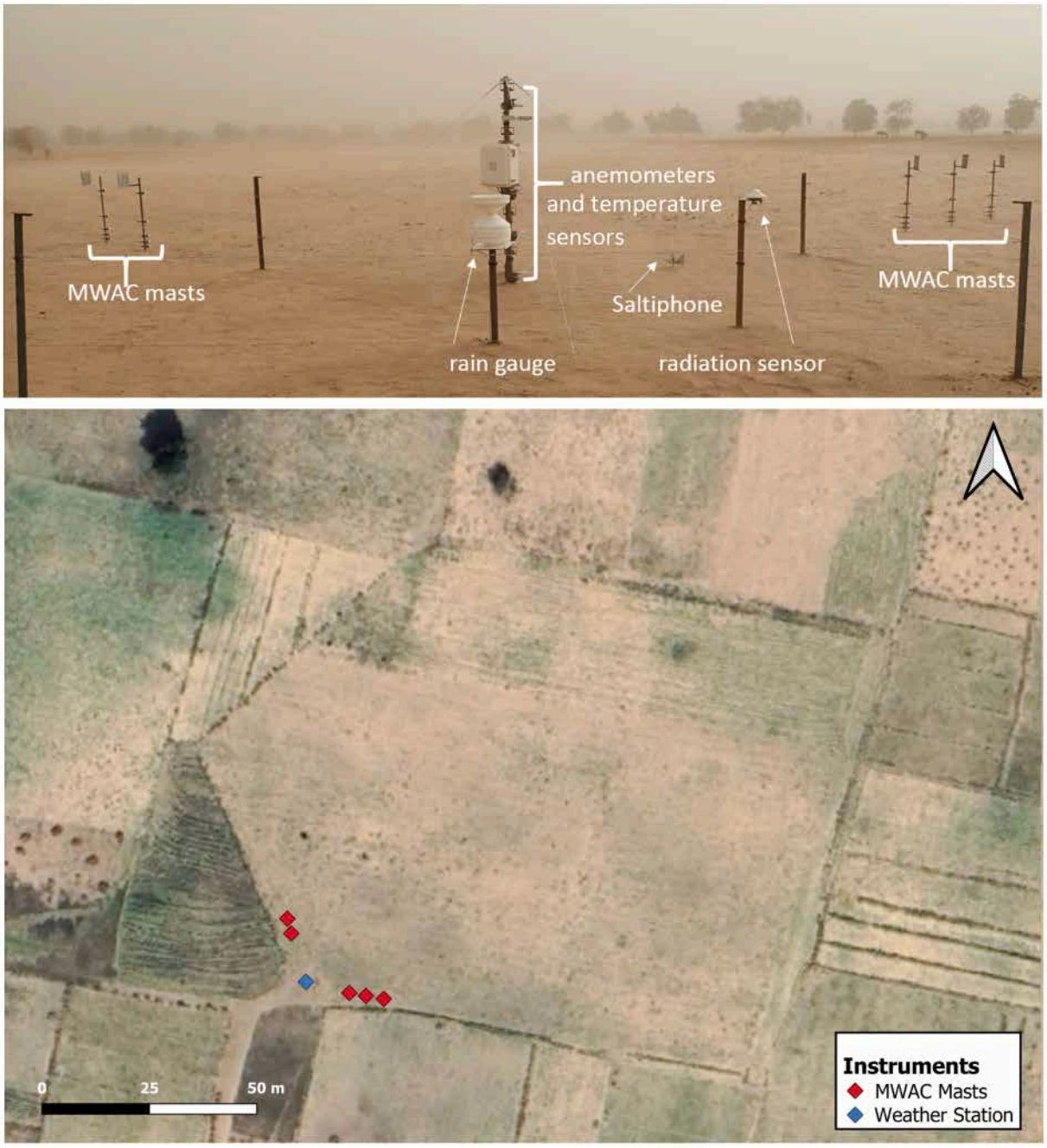

Fig. A1. Experimental setup on the GN0 plot (2020–2021). Top: Annotated picture of the instruments used for measurements (Credit: Jean-Louis Rajot). Bottom: Satellite image of the plot (21 Nov 2021, Credit: Airbus, 2025)

Fig. A1 provides a description of the instruments and setup on the GN0 plot. The mast supporting the anemometers and temperature sensors is what we describe as the "Weather station" on following figures. For the other setups (Fallows, Millet plots), we set the rain gauge, saltiphone and radiation sensor on only one plot each year as we assume that these measurements will be the same on all plots (excepted for the saltiphone count which depend of the surface state of the plot).

Fig. A2 is a satellite image of the fallow plots. On each plot (divided by the dashed red line), the weather station is accompanied by 3 MWAC masts while 2 other are located on the borders of the plots in order to monitor incoming sediments on each plots.

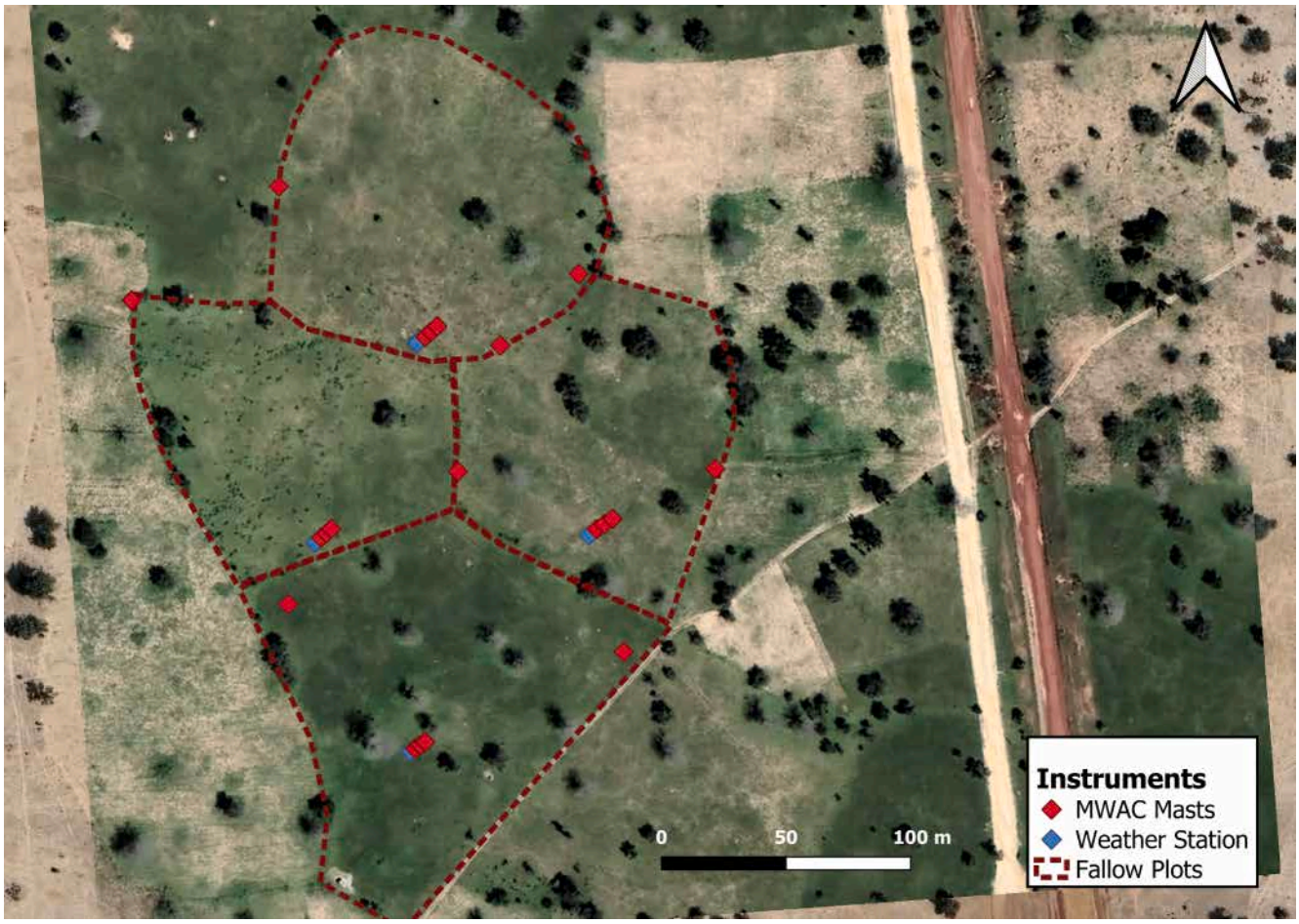

Fig. A2. Satellite image of the experimental setup of the Fallows (2022–2023). From top to bottom, left to right, fallows are F1,F2,F3 and F4. Rain gauge, saltiphone and radiation sensor were placed on F1. (10 October 2022, Credit: Maxar) Technologies, 2025)

Fig. A3 describes the Millet plots. On each plot the weather station is accompanied by 5 MWAC. Grass strips are located between each plot to prevent sediments from entering each plots. These grass strips are at least 10 m wide and were devised by letting weeds develop freely around the plots. The weeds reach 20 cm at the end of the rainy season and degrades over the dry season. The grass strips proved to be efficient in trapping sediments entering and exiting the plots, as shown in Fig. A3.b, the lighter part of the strips are accumulated aeolian sediments.

On each plots, MWAC masts were positioned downwind, in order to measure sediments coming only from the plot (e.g. Fig. A.3.b). This was possible as winds generating most of the aeolian flux take place between February and July.During this period, the wind direction is contained in the 330-60° directions (Fig. 3 and Appendix B, figure B3).

(a)

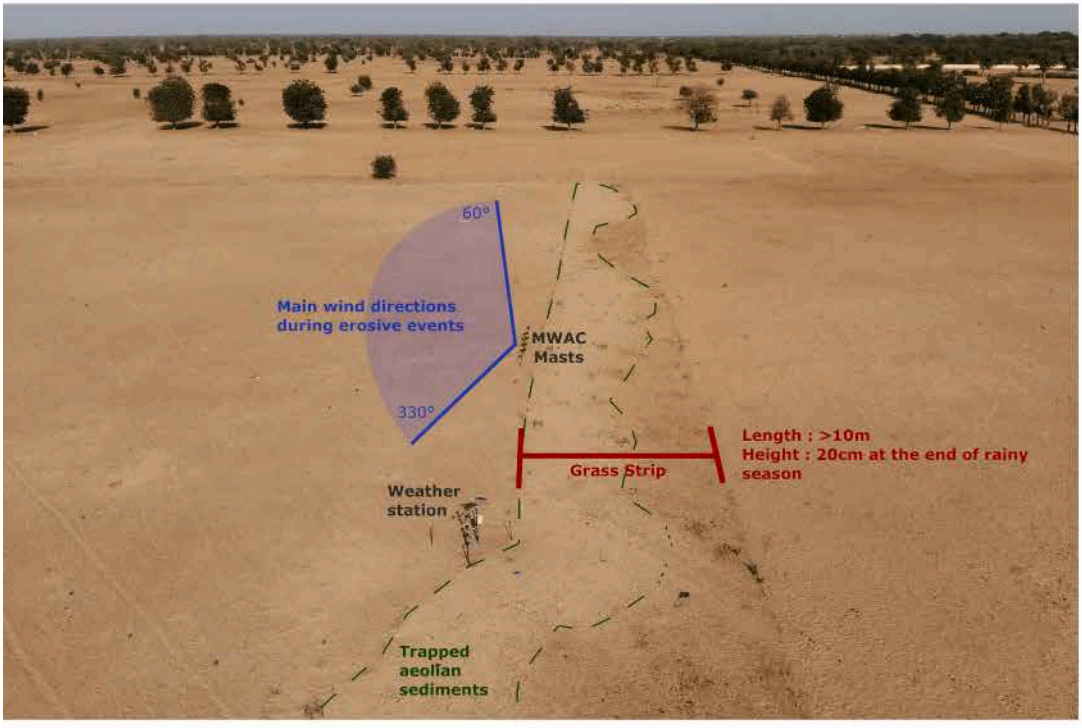

(b)

Fig. A3. Experimental setup on the Millet plots (2023–2024). a) Satellite image of the plots, from top to bottom M4,M3,M2 and M1. Rain gauge, saltiphone and radiation sensor were placed on M4. (12 March 2025, the plots remained instrumented in the same way, Credit: Airbus, 2025). b) Drone photography of M2 highlighting the instrumental setup as well as the role of grass strips in trapping aeolian sediments.

Appendix B. . Meteorological data

The INDAAF weather station in Bambey is located less than 2 km away (14°42′N, 16°28′O) from the experiment site in Bambey. This station provides among other rainfall, temperature and wind measurements at 6 m (Marticorena et al., 2021). INDAAF temperature and wind speed time series are provided in figure B1 for the complete duration of the study. Fig. B2 compares rainfalls time series provided by the INDAAF weather station with on field measurements. Similar patterns and quantities of rainfalls are recorded on the field and by the INDAAF station, and difference in annual precipitation can be either attributed to different sampling dates (the instrumentation of the plots can begin after the first rains, hence the missing events), except for the fallow plots which were located in Ndem, 10 km north of the other plots and of the INDAAF station. The dry spells (over 20 days with less than 20 mm of rain), which have a major role on crop yields (Fall et al., 2021), were consistents between the fields measurements and the INDAAF station.

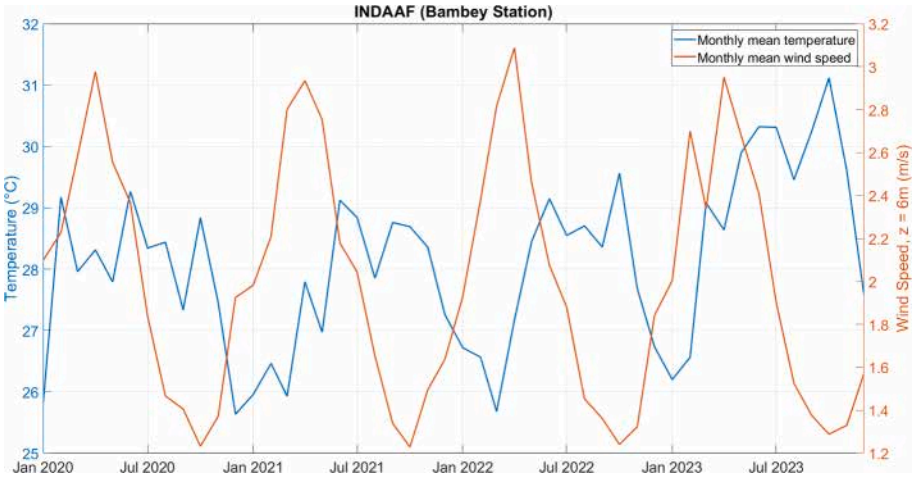

Fig. B1. Monthly mean temperature and wind speed at 6 m, INDAAF weather station, Bambey.

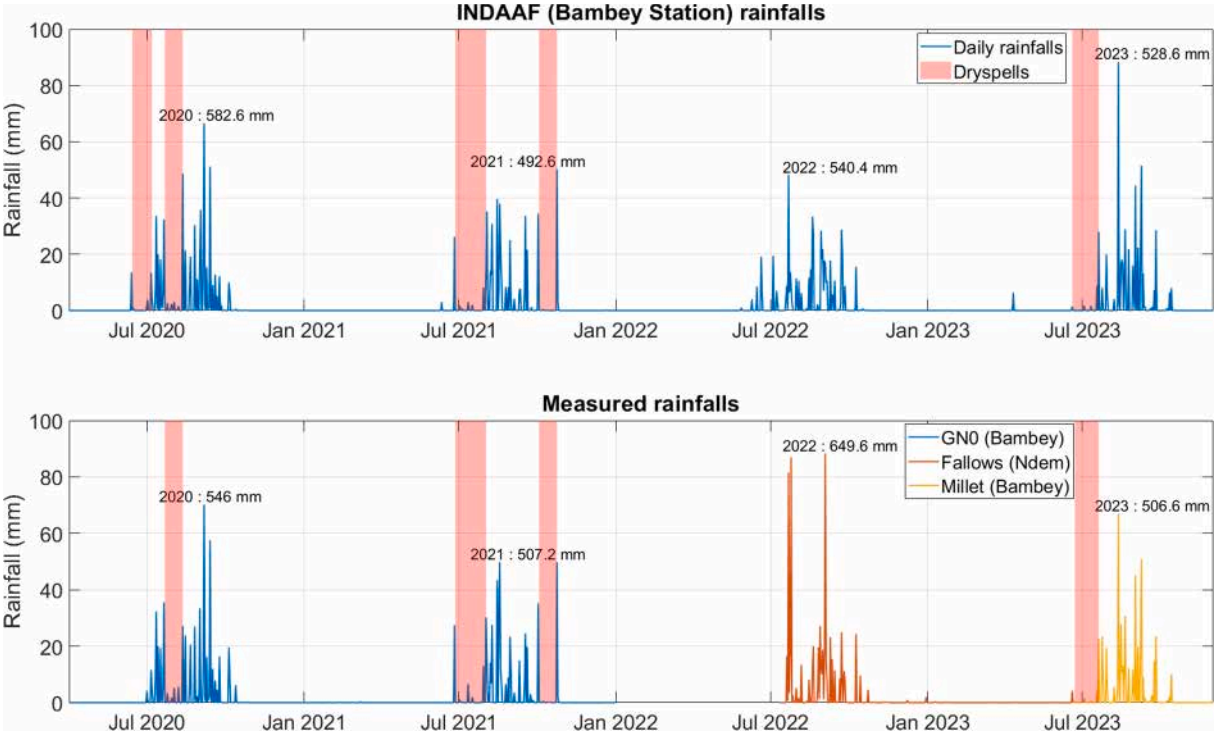

Fig. B2. Daily rainfalls from 2020 to 2023. Top panel: INDAAF recordings, area shaded in red correspond to dry spell periods. Bottom panel: On field measurements, the blue and yellow lines are daily rainfalls in Bambey, while the orange line is daily rainfall in Ndem, 10 km away from Bambey and the INDAAF station.

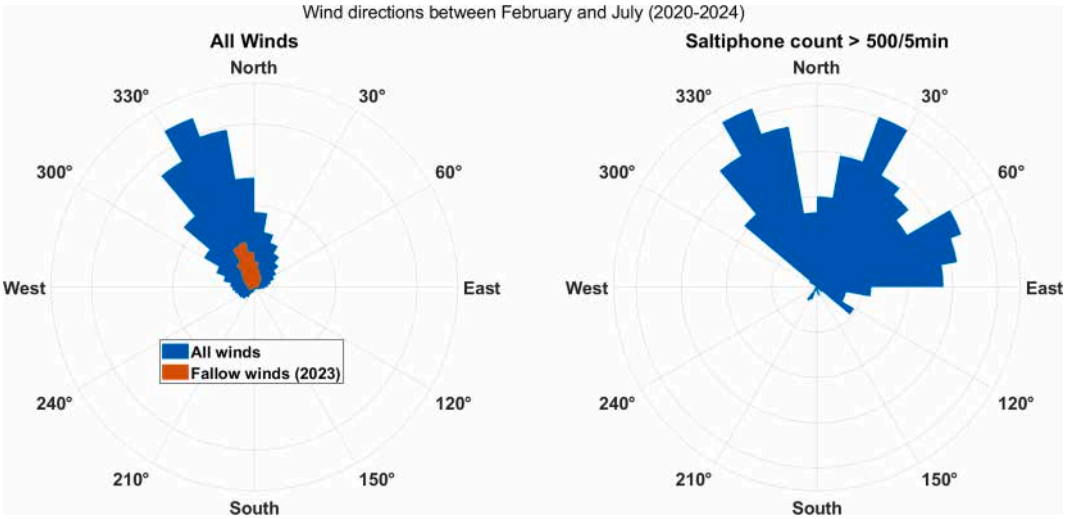

Fig. B3. Wind directions recorded between February (included) and July (excluded, 2020 to 2024. Left panel displays all winds measurements in blue, measurements for F1 (2023) in orange. Right panel displays wind directions coincidental to strong saltiphone measurements.

Fig. B3 displays the main wind directions between February and July, when most of the erosive events take place. Main "erosive" directions are identified by selecting wind direction coincidental to a strong saltiphone measurements (>500 saltiphone counts in 5 mins). The 330°, 30° and 60° directions seem to generate the most flux, while overall, most recorded winds originate from 330°. As almost no horizontal flux was recorded on the fallows, it was not possible to display the "erosive" directions on these plots.However, fallows exhibit the same distribution of wind directions during this period.

In order to estimate the differences in meteorological conditions between the fallow site in Ndem and the other plots in Bambey. We compared fallows rainfall with INDAAF rainfalls (figure B4, left panel) and the wind speed anomaly of fallows (compared to on field measurements in Bambey) with July 2022-June 2023 INDAAF anomaly (figure B4, right panel). Despite being located north of the Bambey site, rains measured on the fallow site are significantly greater than the ones recorded by the INDAAF station (Fallows: 649.6 mm, INDAAF: 540 mm). The difference seems to have been caused by several strong events in July and August happening in Ndem but not in Bambey, the overall dynamic of rainfalls remain however similar between the two sites.

Wind speeds measured on the fallow sites were significantly lower than the ones measured at the same time of year on other plots (Fig. B4, right panel). This is most likely due to the geographic location of the site as INDAAF measurements don't exhibit the same drop in average wind speed from July 2022 to June 2023. This may have been caused by the higher density of trees on the fallow site, creating obstacle and decreasing the wind speed, event at 1.9 m (See appendix A, figure A2).

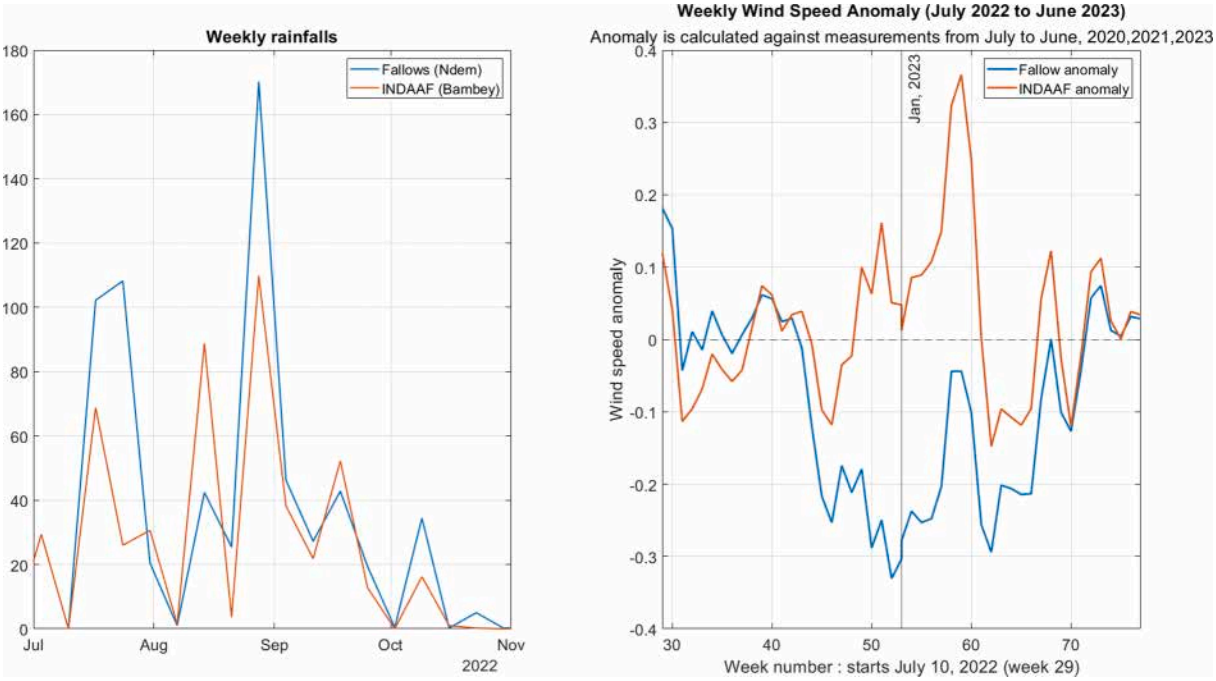

Fig. B4. Fallow site (Ndem) and Bambey meteorological conditions comparison. Left panel: Weekly rainfalls on F1 (Ndem) and the INDAAF station (Bambey) from July to November 2022. Righ panel: Wind speed anomaly (Weekly wind speed – average wind speed during this week)/ average wind speed during this week for fallows (average is calculated with measurements on GN0 and millet plots) and for the INDAAF station (average is calculated with 2020 to 2024 data, excluding data from July 2022 to June 2023).

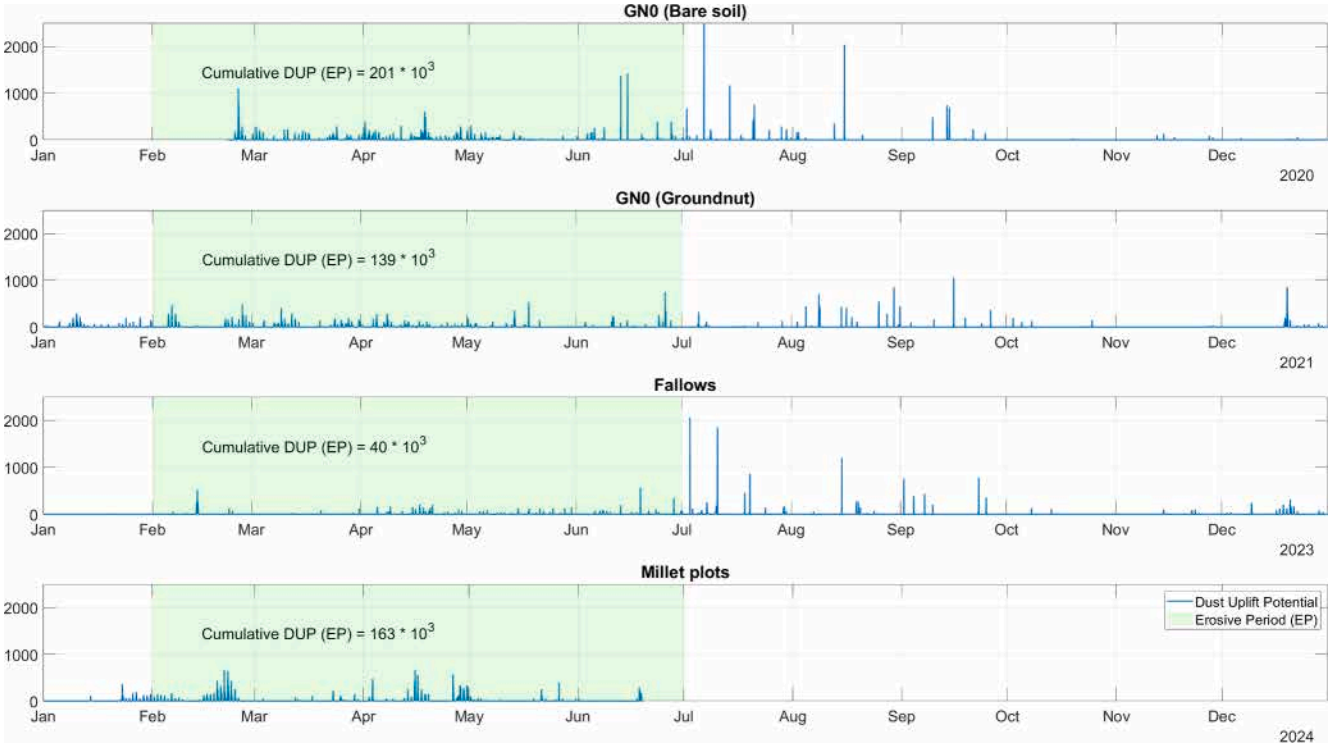

Fig. B5. Dust uplift potential on all studied plots. The erosive period (EP) was defined as the time period between February 1st and July 1st, when most of the horizontal flux generation takes place.

Appendix C. . Vegetation measurements details

Table C1
Vegetation measurements details

Plot	Frequency of non-destructive sampling	Sampling size	Sampling category	Frequency of destructive sampling (rainy season/dry season)	Sampling size	Sampling categories	Max mean total biomass (kg/ha)
Groundnut (2021)	18 measures between aug and nov 2021 for groundnut	1 m2 * 8	Height	15 measures between aug and nov 2021, 9 measures of weed biomass during dry season	1 m2 * 8	Groundnut (roots, stems, leaves, flowers, pods)Total herbaceous vegetation	678
Fallows (2022)	Weekly	2*1.5 m2 * 25 for each plot	Height, cover (photography), trampling	Monthly	1 m2 * 5	Millet residues (from the previous year), green herbaceous vegetation, dry herbaceous standing vegetation, dry herbaceous litter	811
Millet (2023)	Weekly	1.8*0.9 m2 * 28 for each plot	Height, cover (photography), trampling	Every two weeks / monthly	1.8*0.9 m2 * 6	Millet (leaves, stems, cobs), cowpea (leaves, stems, pods), weeds (green, dry), residues	2040

Appendix D. . Groundnut parametrization

STICS' groundnut parametrization is a parametrization of the short-cycle Fleur 11 variety (90–100 days) which is representative of other short-cycle varieties that are mainly used in the groundnut basin. The calibration is based on a set of 65 experiments (35 for calibration et 30 for evaluation) on 3 sites (Bambey, Nioro, Niakhar) in the groundnut basin and multiple years and types of practices.

The model already proved to be able to simulate legume's nitrogen fixation (Falconnier et al., 2019, Traoré et al., 2022) and a prototype of groundnut parametrization in STICS based on the calibration of other models (Ricome et al., 2017, Naab et al. 2004) and experimental measures in Senegal (Agbohessou et al., 2022) was the base used for the calibration. Following the methodology described in Falconnier et al., 2019, calibration was made through literature review, parameter determination from experimental data and optimization (manual calibration). Finally, 37 parameters were fixed (9 through literature review, 3 from field measurements and 25 from manual calibration), describing plant phenology, biomass development, yield formation, and nitrogen fixation and uptake.

Measurements of LAI, aboveground and fruit biomass, and soil water content were made to evaluate to calibrate and evaluate the parametrization.

During this calibration stage, the model showed an overestimation of aboveground biomass when observed biomass is low, yet agreed with the

overall dynamic of the observations. nRMSE values for aboveground and fruit biomass ranged respectively from 39.5 to 45 % and 38.3 to 51 %. High nRMSE values were also found for LAI simulations, the discrepancy can be caused by the assumption that LAI stops growing after the start of leaf senescence. Biomass is not impacted by stress during flowering, which does not match the observations and leads to biomass overestimation in water-stressed conditions. This calibration led nonetheless to a satisfying agreement between observed and simulated parameters, as well as an accurate representation of the plant phenology.

Appendix E. . Dry module for STICS

While the STEP model provides an accurate simulation of degrading herbaceous vegetation, the STICS model handles the crop from sowing to harvest. To model the degradation of millet residues left on the plot, a dry vegetation submodel is added to STICS, based on the addition of the same submodel on the SARRAH model (Pierre et al., 2015). The dry vegetation submodel describes the decay of standing millet residues caused by herbivory and climatic factors (decomposition, abrasion). It also deals with the transformation of standing vegetation into litter caused by wind and trampling. Finally, litter decay is also modeled through herbivory, burying through trampling and decomposition.

Because this submodel treats differently stem biomass from leaves biomass and STICS does not accurately separate the two, the final aboveground biomass minus the harvested organs is manually separated into two compartments:

$$B_{standing,leaves}(t=0) = \left(B_{aboveground}(t=harvest) - B_{fruit}(t=harvest)\right)*percleaves \quad \text{(E.1)}$$

$$B_{standing,stems}(t=0) = \left(B_{aboveground}(t=harvest) - B_{fruit}(t=harvest)\right)*(1-percleaves) \quad \text{(E.2)}$$

Where percleaves = 0.4, based on observations at harvest for millet.

Then the degradation is handled through differential equations described in Pierre et al., 2015:

$$\frac{dB_{standing,leaves}}{dt} = -\left(K_{degrad,up} + K_{trampling} + K_{ingest}\right)*B_{standing,leaves} \quad \text{(E.3)}$$

$$\frac{dB_{standing,stems}}{dt} = -\left(K_{degrad,up} + K_{trampling}\right)*B_{standing,stems} \quad \text{(E.4)}$$

$$\frac{dB_{litter,leaves}}{dt} = K_{trampling}*B_{standing,leaves} - K_{degrad,lit}*B_{litter,leaves} \quad \text{(E.5)}$$

$$\frac{dB_{litter,stems}}{dt} = K_{trampling}*B_{standing,stems} - K_{degrad,lit}*B_{litter,stems} \quad \text{(E.6)}$$

Where $K_{degrad,up} = 0.001$ d-1 is the degradation from physical and abiotic factors for standing vegetation, $K_{trampling} = 0.003$ * livestock d-1, the livestock is expressed in Tropical Livestock Unit per km2 or TLU/km2, $K_{ingest} = 0.005$*livestock d-1 and $K_{degrad,lit} = 0.011$ d-1. The coefficients are derived from field studies (Schlecht and Hiernaux, 2001; Hiernaux and Ayantunde, 2004; Kergoat et al., 2015), STEP model degradation values (Delon et al., 2015), and coefficient of litter degradation taken from Abdourhamane Touré et al. (2011).

Appendix F. . Model calibration

F.1. Biomass simulation

For the GN0 plot simulation, the output from the crop model STICS shows a strong overestimation (Fig. 8) of the aboveground biomass as it reaches over 300 gDM/m^2 for each simulated year, while the maximum observed biomass for year 2021 was less than 100 gDM/m^2 at best. This difference is explained by STICS difficulty to simulate highly water and nutrient stressed growing conditions, as was the case in this experiment. However, the phenology of the groundnut was accurately simulated, as fructification and maturity predicted and observed dates were close (fructification was predicted on September 19 and observed between September 11 and September 20, maturity was predicted on November 10, right before the actual harvest on November 16).

Weeds on the field were simulated using the STEP model (Fig. F.1.) and the final biomass was weighted according to the effective area that could be covered by weeds during the cropping season. We use a RMSE minimizing optimization method to first set the value of the conversion efficiency parameter ε, and then the value of the grazing pressure, in TLU/km^2 (Tropical Livestock Unit per km^2) which affects the degradation of the plot vegetation. The final values were 3.6 g/MJ for ε and 5 TLU/km^2. This grazing pressure is on the lower range of Sahelian estimations but is consistent with animal presence over low fertility areas (Turner and Hiernaux 2002; Pierre et al., 2015; Audouin et al., 2017).

Table F1
STEP Model parameter calibration for each fallow.

Fallow	ε (g/MJ)	TLU/km^2
F1	2.98	10
F2	3.19	5
F3	2.90	10
F4	3.20	5

Following the same method as described for GN0 weeds, individual calibration was made for each fallow, results are shown in Table F.1.. ε is consistent with what is known of each fallow (F2 and F4 are older fallows, presumed to be more

fertile). Estimated maximum value of grazing pressure for each plot through biomass optimization was between 5 and 10 TLU/km^2. The output of the STEP model after calibration is in very good agreement with observed biomass (Fig. F.1.), especially for standing (green and dry) biomass. Litter biomass is slightly underestimated during the beginning of the dry season (from October to February). The degradation dynamics and proportion between lying and standing biomass is accurately simulated.

Table F2
STICS and STEP model parameter calibration for millet plots.

Millet field	ε (STEP)	TLU/km^2 (STEP)	TLU/km^2 (dry module)	Nitrate modulation (STICS)
M1	3.89	25	2	22 %
M2	3.51	20	No dry module	2 %
M3	3.61	10	3	0 %
M4	2.80	10	No dry module	0 %

For each millet plot, vegetation was simulated through the STICS model for millet development and the STEP model for weed development and degradation (Same as fallows and GN0).The dry millet degradation module was added to STICS for M1 and M3 where millet residues were left on field. For M2 and M4, nearly all residues were collected and the only simulated cover after harvest is weeds.

While the values of grazing pressure are in the expected range of values and are consistent with each other (from 10 to 25 TLU/km^2), the grazing pressure on M1 (25 TLU/km2) is higher than other values and the estimated grazing pressure for millet degradation with the dry module (Table F.2.). This might be caused by the stark decrease of weed vegetation on M1 compared to other millet plots, which can also be caused by non-animal factor such as human interaction. Regarding millet, the STICS model was calibrated through the modulation of the nitrogen content of the plots to estimate soil fertility. The baseline was established with default STICS soil nitrogen content (NO_3 ranging from 15 to 20 kg/ha and NH_4 ranging from 4 to 10 kg/ha depending on soil depth, which is the required N amount for millet culture, Bationo and Ntare, 2000; Kidron et al., 2009) and was modulated to better fit our observations. Heavy nitrogen stress was necessary to accurately reproduce the observed biomass, which is consistent with soil measurements made on the plot in 2021, and overall the low input agriculture of Senegal, especially in the study area.

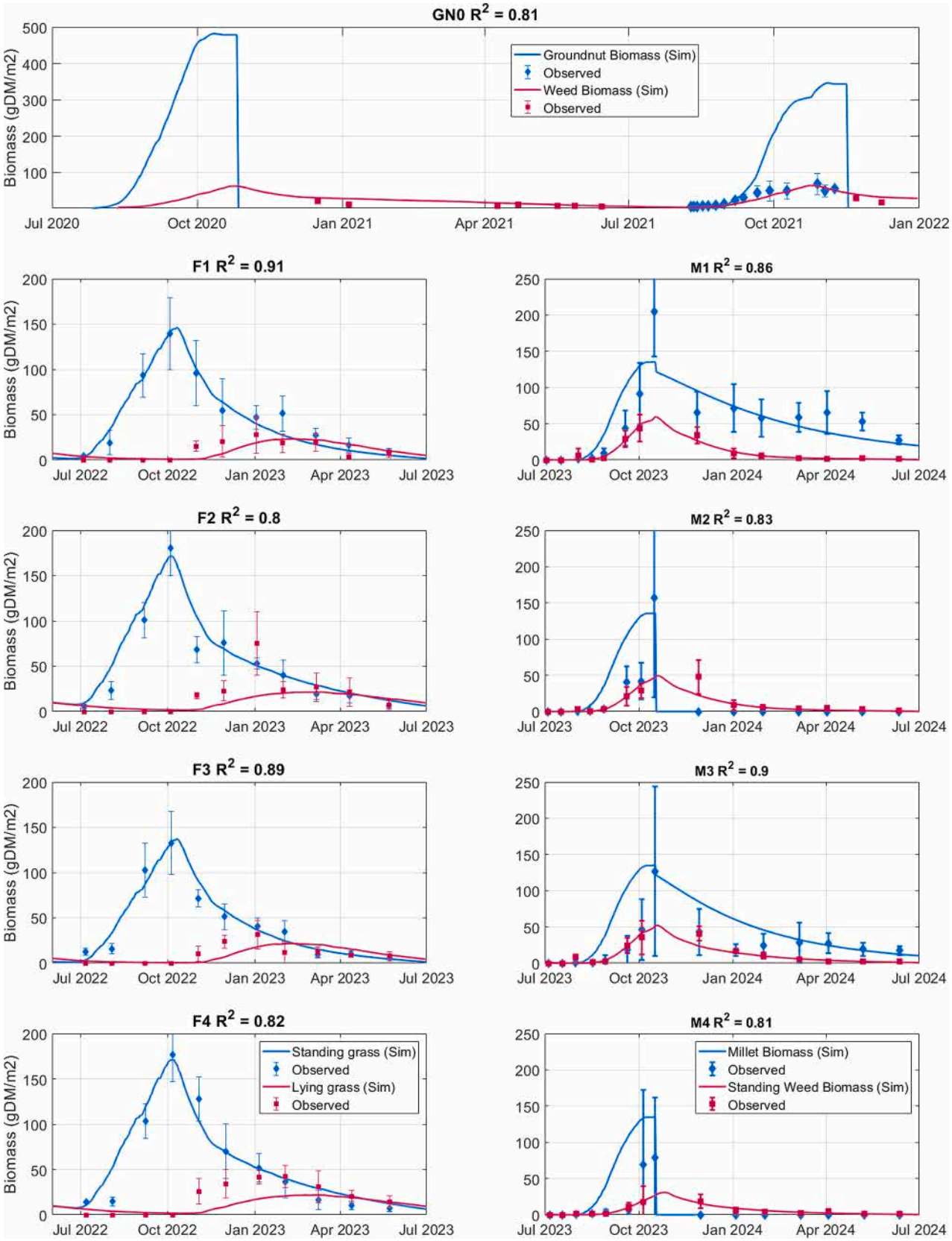

Fig. F1. Top Panel: Groundnut and weeds biomass on plot GN0. R^2 is calculated on the total vegetation biomass. Left: Weed biomass on fallows, standing vegetation is green and litter is brown, Right: Millet (green) and weed (brown) biomass on millet plots. Observations are represented with standard deviations (squares), simulations are represented with a line. R^2 is calculated on the total vegetation biomass.

Though maximal millet biomass is accurately simulated by STICS, the simulated millet growth is very early in comparison to our observations. However, this model bias will not affect wind erosion simulation as almost no horizontal flux is generated during the period of the year in this part of

the Sahel.

F.2. Aerodynamic roughness parametrization

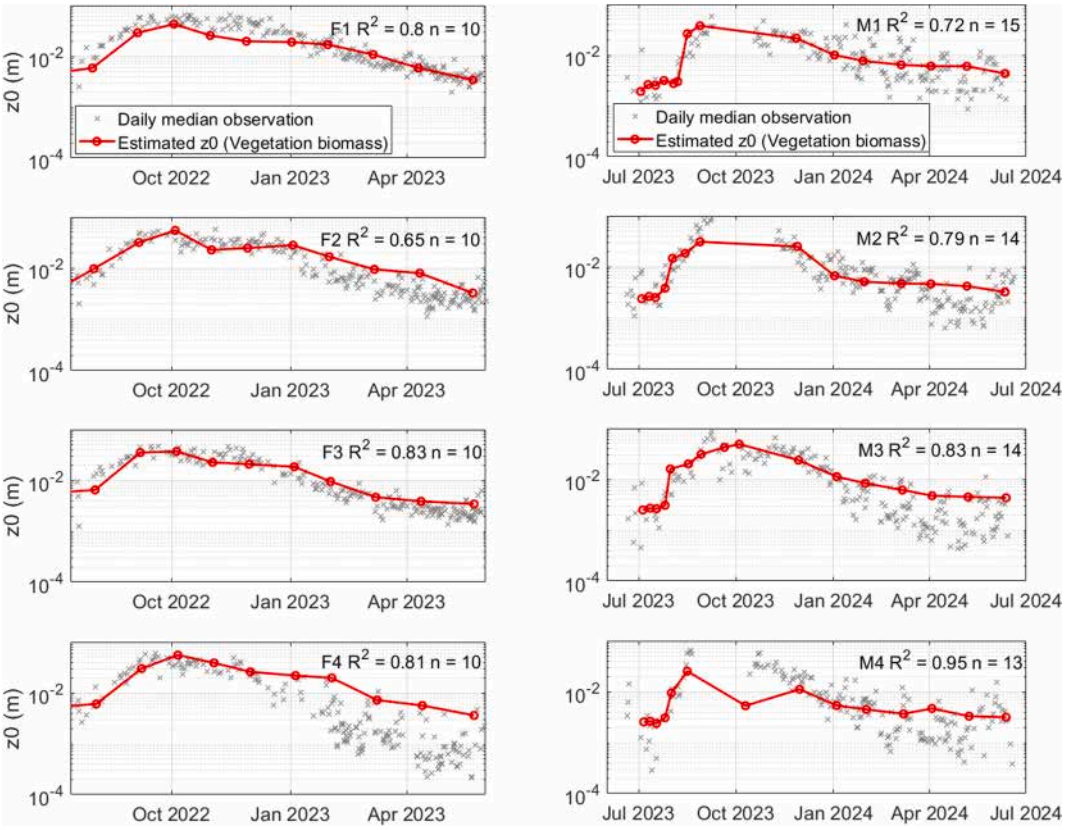

Fig. F2. z_0 parametrization for fallows (left) and millet plots (right). R^2 is calculated between all z_0 estimations and the median observed value of z_0 in a 30-day window around the estimations.

For each type of land cover, we use a parametrization linking aerodynamic roughness length z_0 to a vegetation variable.

For herbaceous vegetation growing on fallows and for weeds on crops, we adapted a previous parametrization from Pierre et al. (2015) designed for rangeland in Central Mali by regressing z_0 values against monthly observations of vegetation aerial mass. The updated equation is the following:

$$z_0 = 0.0003 * B_{standing} + 0.00015 * B_{litter} \quad \text{(F.1)}$$

with the biomass B expressed in $g.m^{-2}$.

For 41 measures, equation (F.1). gave a R^2 of 0.65 on our fallow dataset. z_0 parametrizations based on biomass observations are presented in Fig. F.2.

Similarly, by fitting the biomass measurements of groundnut against the z_0 observations, the following equation is obtained:

$$z_0 = 5.1 * 10^{-4} * B_{groundnut} + z_{0s} \quad (R2 = 0.76,\ n = 15) \quad \text{(F.2)}$$

At the beginning of the growing season, multiple weedings occurred to eliminate the development of competing herbaceous vegetation. Weeds, however, still developed in the later months of the rainy season (September – October) and provided the only soil cover after groundnut harvest. At the beginning of the dry season of 2020, around 40 % of the field was still partially occupied by weeds. It is then necessary to consider them when simulating the z_0 time series outside the groundnut growing season. The relation between weed biomass and aerodynamic roughness length (Eq. (F.1).) is the same as the one used on fallows. When using the relationship on the observed weed biomass on the groundnut field during the 2020–2021 dry season, we obtain $R^2 = 0.98$, for $n = 7$. The overall parametrization is a maximum between the groundnut and weed parametrization, it scores an R^2 of 0.81 for $n = 24$ (Fig. F.3).

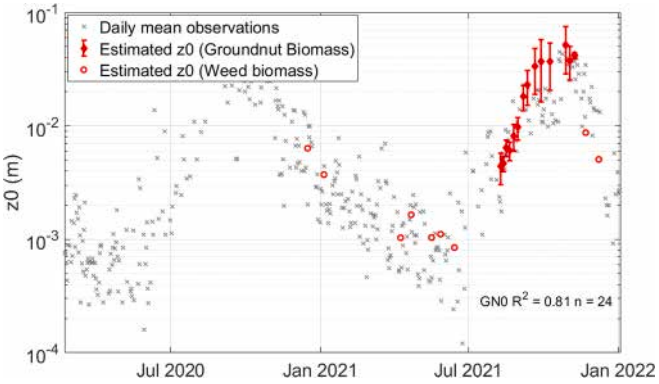

Fig. F3. z_0 parametrization compared to observations for GN0. z_0 estimations for groundnut and weeds biomass are respectively derived from equations 8 and 7. R^2 is calculated between all z_0 estimations and the mean observed value of z_0 in a 30-day window around the estimations.

Millet parametrizations were proposed in previous studies, linking roughness either to millet height (Pierre et al., 2015) or biomass (Pierre et al., 2018).

Biomass-based parametrization proved to be more efficient in estimating z_0 values because biomass is better correlated to cover density than height. However, the relationship between biomass and roughness changes before and after the harvest when the millet stems degrade and fall, affecting the value z_0 because of changes in geometry of vegetation cover rather than in its biomass. Also, the development of weeds during and after cropping plays a non-negligible role in roughness (Bielders et al., 2004).

Before harvest, the logarithm of millet biomasses after the exclusion of outlier masses was regressed against the average z_0 value (7-day average centered on measured date).

$$z_0 = 7.1*10^{-3}*ln(B_{millet}) + 2.15*10^{-2} \quad \text{(F.3)}$$

Where B_{millet} is the total aerial millet biomass.

After the harvest, the z_0 parametrization takes into account millet residues biomass and herbaceous biomass.

$$z_0 = 4.4*10^{-5}*B_{millet} + 4.7*10^{-4}*B_{weeds} + 0.001 \quad \text{(F.4)}$$

Where B_{weeds} is the total aerial weed biomass.

Table F3
Summary of z_0 parametrizations for each type of modeled vegetation. All relations are empirical. Biomass units is in $g.m^{-2.}$

Land cover	Used vegetation variable	z_0 estimation method	Equations
Groundnut	Groundnut aboveground biomass (agb), herbaceous agb (standing, litter)	Maximum between function of groundnut biomass and function of weed biomass.	$z_0 = 5.1*10^{-4}*B_{groundnut} + z_{0s}$ $z_0 = 0.0003*B_{standing} + 0.00015*B_{litter}$ (adapted from Pierre et al. (2015))
Fallows	Herbaceous agb (standing, litter)	Function of weed biomass	$z_0 = 0.0003*B_{standing} + 0.00015*B_{litter}$ (adapted from Pierre et al. (2015))
Millet	Millet agb, herbaceous agb (standing litter)	Before harvest, maximum between function of millet aboveground biomass and function soil residues cover	Before harvest: $z_0 = 7.1*10^{-3}*ln(B_{millet}) + 2.15*10^{-2}$ After harvest: $z_0 = 4.4*10^{-5}*B_{millet} + 4.7*10^{-4}*B_{weeds} + 0.001$
		After harvest, maximum between function of millet and herbaceous biomass and function of soil residues cover	$z_0 = 0.0012ln(f_{cv}) + 0.0013$ (Abdourhamane Touré et al., 2011)

Litter cover also affects the roughness z_0 and is considered through the equation proposed in Abdourhamane Touré et al. (2011):

$$z_0 = 0.0012 * ln(f_{cv}) + 0.0013 \quad \text{(F.5)}$$

with f_{cv} the fraction of soil surface covered by vegetation.

The final z_0 value is the maximum between the relevant regressed relation (before or after harvest) and the impact of litter cover, following the methodology described in Pierre et al. (2018).

Finally, the R^2 values from this overall parametrization ranged from 0.72 to 0.95, for an overall 0.73 on all plots ($n = 56$). The correlation between observed z_0 values and estimated ones from biomass measurements excludes values calculated in September and October as z_0 observations were too scarce during this period to be reliable. A summary of all z_0 parametrization is presented in Table F.3.

F.3. Simulated aerodynamic roughness length

Using the parametrization from section F.2. and biomass simulation, we modeled an aerodynamic roughness length time-serie z_{0sim} for the groundnut plot, fallows, and millet plots. Correlation and RMSE between observed and simulated z_0 values are reported in Table F.4.

For the groundnut plot (GN0), from February to July 2020, the value of z_0 is set to z_{0s} to account for field clearing. After this date, z_0 is set to the maximum of the z_0 derived from groundnut and the one derived from weeds biomass. From sowing to harvest, the groundnut cover is the main driver

of z_0, and overestimation of groundnut biomass thus also leads to an overestimation of z_0 around vegetation maximum (z_0 max 2020 = 36 cm, z_0 max 2021 = 26 cm). After harvest, z_0 is derived from the weeds biomass and a better agreement is found between observed and simulated z_0 values (Fig. F.4.) The degradation of weeds over time allows for a good description of the decline in z_0 values from harvest to beginning of the next rainy season. Overall, this parametrization gives satisfying results (R^2 = 0.6, n = 392), especially between January and June 2021 when most of the horizontal flux was generated.

Table F4
Correlation between observed and simulated z_0.

Plot	GN0	F1	F2	F3	F4	M1	M2	M3	M4
n	392	237	215	210	206	177	205	201	179
R^2	0.6	0.88	0.75	0.85	0.86	0.61	0.8	0.58	0.67
RMSE	0.061	0.011	0.007	0.004	0.008	0.009	0.008	0.012	0.009

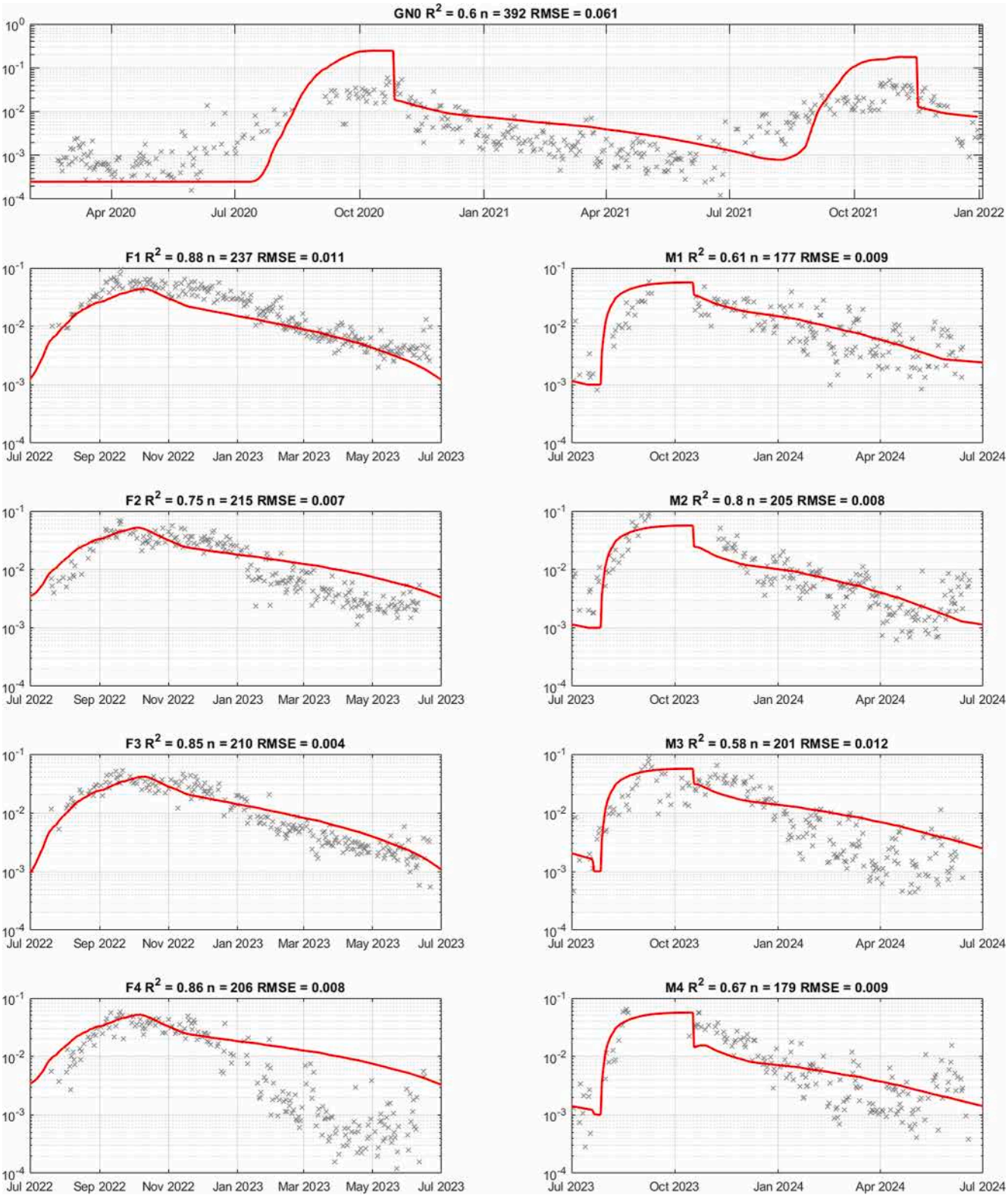

Fig. F4. {z0 simulation and daily estimations} Aerodynamic roughness length simulations (red line) and daily estimations (grey crosses) for GN0 (top), fallows (left) and millet plots (right).

A strong agreement between observed and simulated z_0 values has been found for fallows with R^2 ranging from 0.75 (n = 215) to 0.88 (n = 237). From July to October, the increase of z_0 is explained by vegetation growth. During the dry season, z_0 is influenced by the decrease of herbaceous biomass and the transformation of standing dry biomass into litter.

For the millet plots, the z_0 time-series derived from biomass value are in good agreement with observed z_0, with R^2 values ranging from 0.58 (n = 201) to 0.8 (n = 205). Millet growth drives the z_0 increase from July to October on all plots. After harvest on plots with residue collection (M2 and M4), z_0's decrease results from weed biomass degradation. z_0 decreases on M1 and M3 where residues left on field are a combination of millet stems and

weed biomass degradation. On both plot, weeds are the main driver of aerodynamic roughness evolution until the middle of the dry season (January) and as weeds continue degrading, millet residues take a more preponderant role. Litter-caused roughness rarely surpasses biomass-caused roughness in our simulations.

Data availabilityi.

Evaluating the impact of different agropastoral practices on wind erosion in western Sahel (Original data) (Mendeley Data)

References

Abdourhamane Touré, A., Rajot, J.L., Garba, Z., Marticorena, B., Petit, C., Sebag, D., 2011. Impact of very low crop residues cover on wind erosion in the Sahel. Catena 85, 205–214. https://doi.org/10.1016/j.catena.2011.01.002.

Abdourhamane Touré, A., Tidjani, A.D., Rajot, J.L., Marticorena, B., Bergametti, G., Bouet, C., Ambouta, K.J.M., Garba, Z., 2019. Dynamics of wind erosion and impact of vegetation cover and land use in the Sahel: a case study on sandy dunes in southeastern Niger. Catena 177, 272–285. https://doi.org/10.1016/j.catena.2019.02.011.

Agbohessou, Y., Audebert, A., Ndour, A., Sokhna Sarr, M., Jourdan, C., Clermont-Dauphin, C., Diatta, S., Leroux, L., Taugourdeau, S., Sanogo, D., Seghieri, J., Delon, C., Roupsard, O., 2022. Using UAV and geostatistics to upscale crop yield in heterogeneous agro-silvo-pastoral system EGU22-11773. DOi: 10.5194/egusphere-egu22-11773.

Agbohessou, Y., Delon, C., Mougin, E., Grippa, M., Tagesson, T., Diedhiou, M., Ba, S., Ngom, D., Vezy, R., Ndiaye, O., Assouma, M.H., Diawara, M., Roupsard, O., 2023. To what extent are greenhouse-gas emissions offset by trees in a Sahelian silvopastoral system? Agric. For. Meteorol. 343, 109780. https://doi.org/10.1016/j.agrformet.2023.109780.

Audouin, É., Vayssières, J., Odru, M., Masse, D., Dorégo, S., Delaunay, V., Lecomte, P., 2017. Chapter 19. Reintroducing livestock to increase the sustainability of village landscapes in West Africa, in: Sultan, B., Lalou, R., Sanni, M.A., Oumarou, A., Arame Soumaré, M. (Eds.), Rural Societies in the Face of Climatic and Environmental Changes in West Africa. IRD Éditions, pp. 375–398. DOi: 10.4000/books.irdeditions.12391.

Aubault, H., Webb, N.P., Strong, C.L., McTainsh, G.H., Leys, J.F., Scanlan, J.C., 2015. Grazing impacts on the susceptibility of rangelands to wind erosion: The effects of stocking rate, stocking strategy and land condition. Aeolian Research 17, 89–99. https://doi.org/10.1016/j.aeolia.2014.12.005.

Badiane, A.N., Diagne, M., Fall, A., Faye, A., Kebe, M., Khouma, M., Sène, M., 2000. Gestion et transformation de la matière organique. Synthèse Des Travaux De Recherches Menés Au Sénégal Depuis 1945. ISRA.

Bationo, A., Ntare, B.R., 2000. Rotation and nitrogen fertilizer effects on pearl millet, cowpea and groundnut yield and soil chemical properties in a sandy soil in the semi-arid tropics, West Africa. J. Agric. Sci. 134, 277–284. https://doi.org/10.1017/S0021859699007650.

Bergametti, G., Marticorena, B., Rajot, J.L., Siour, G., Féron, A., Gaimoz, C., Coman, A., Chatenet, B., Coulibaly, M., Maman, A., Koné, I., Zakou, A., 2020. The respective roles of wind speed and green vegetation in controlling Sahelian dust emission during the wet season. Geophys. Res. Lett. 47, e2020GL089761. https://doi.org/10.1029/2020GL089761.

Bergametti, G., Rajot, J.L., Pierre, C., Bouet, C., Marticorena, B., 2016. How long does precipitation inhibit wind erosion in the Sahel? Geophys. Res. Lett. 43, 6643–6649. https://doi.org/10.1002/2016GL069324.

Bielders, C., Rajot, J.L., Karlheinz, M., 2004. L'érosion éolienne dans le Sahel nigérien : influence des pratiques culturales actuelles et méthodes de lutte. Sécheresse 15, 1–14.

Bielders, C., Vrieling, A., Rajot, J., Skidmore, E., 2001. On-farm evaluation of field-scale soil losses by wind erosion under traditional management in the Sahel. In: Soil Research for the 21ste Century, Hawaii 2001. - [S.l.] : [s.n.], 2001. DOi: 10.13031/2013.4585.

Bielders, C.L., Michels, K., Rajot, J.-L., 2000. On-farm evaluation of ridging and residue management practices to reduce wind erosion in Niger. Soil Sci. Soc. Am. J. 64, 1776–1785. https://doi.org/10.2136/sssaj2000.6451776x.

Bielders, C.L., Rajot, J.-L., Amadou, M., 2002. Transport of soil and nutrients by wind in bush fallow land and traditionally managed cultivated fields in the Sahel. Geoderma 109, 19–39. https://doi.org/10.1016/S0016-7061(02)00138-6.

Blanco-Canqui, H., Wortmann, C., 2017. Crop residue removal and soil erosion by wind. J. Soil Water Conserv. 72, 97A–104A. https://doi.org/10.2489/jswc.72.5.97A.

Brandt, M., Romankiewicz, C., Spiekermann, R., Samimi, C., 2014. Environmental change in time series – an interdisciplinary study in the Sahel of Mali and Senegal. J. Arid Environ. 105, 52–63. https://doi.org/10.1016/j.jaridenv.2014.02.019.

Brisson, N., Gary, C., Justes, E., Roche, R., Mary, B., Ripoche, D., Zimmer, D., Sierra, J., Bertuzzi, P., Burger, P., Bussière, F., Cabidoche, Y.M., Cellier, P., Debaeke, P., Gaudillère, J.P., Hénault, C., Maraux, F., Seguin, B., Sinoquet, H., 2003. An overview of the crop model stics. Eur. J. Agron. 18, 309–332. https://doi.org/10.1016/S1161-0301(02)00110-7.

Buldgen, A., Piraux, M., Dieng, A., Compère, R., 1993. Mise au point de techniques d'embouche bovine villageoise dans le bassin arachidier sénégalais. Revue Mondiale De Zootechnie 27–34.

Casenave, A., Valentin, C., 1992. A runoff capability classification system based on surface features criteria in semi-arid areas of West Africa. J. Hydrol. 130, 231–249. https://doi.org/10.1016/0022-1694(92)90112-9.

Chi, W., Zhao, Y., Kuang, W., He, H., 2019. Impacts of anthropogenic land use/cover changes on soil wind erosion in China. Sci. Total Environ. 668, 204–215. https://doi.org/10.1016/j.scitotenv.2019.03.015.

Cissokho, R., 2011. Développement d'un indice de vulnérabilité à l'érosion éolienne à partir d'images satellitales, dans le bassin arachidier du sénégal. Cas De La Région De Thiès. Université de Montréal.

Darmenova, K., Sokolik, I.N., Shao, Y., Marticorena, B., Bergametti, G., 2009. Development of a physically based dust emission module within the Weather Research and Forecasting (WRF) model: assessment of dust emission parameterizations and input parameters for source regions in Central and East Asia. J. Geophys. Res. 114, D14201. https://doi.org/10.1029/2008JD011236.

De Rosnay, P., Gruhier, C., Timouk, F., Baup, F., Mougin, E., Hiernaux, P., Kergoat, L., LeDantec, V., 2009. Multi-scale soil moisture measurements at the Gourma meso-scale site in Mali. J. Hydrol. 375, 241–252. https://doi.org/10.1016/j.jhydrol.2009.01.015.

Delon, C., Mougin, E., Serça, D., Grippa, M., Hiernaux, P., Diawara, M., Galy-Lacaux, C., Kergoat, L., 2015. Modelling the effect of soil moisture and organic matter degradation on biogenic NO emissions from soils in Sahel rangeland (Mali). Biogeosciences 12, 3253–3272. https://doi.org/10.5194/bg-12-3253-2015.

Diallo, S., Diallo, M.D., Nacro, H.B., Traoré, S.A., N'Diaye, A., 2017. FACTEURS EDAPHIQUES ET DYNAMIQUE DES TERRES AGRICOLES DANS LE BASSIN ARACHIDIER DE LA REGION DE THIES (SENEGAL) : EFFICACITE DES STRATEGIES D'ADAPTATION DES POPULATIONS 22.

Doso Jnr, S., 2014. Land degradation and agriculture in the Sahel of Africa: causes, impacts and recommendations. JASA 03, 67–73. https://doi.org/10.14511/jasa.2014.030303.

Elliot, P., 1958. The growth of the atmospheric internal boundary layer. Eos Trans. AGU 39, 1048–1054. https://doi.org/10.1029/TR039i006p01048.

Falconnier, G.N., Journet, E.-P., Bedoussac, L., Vermue, A., Chlébowski, F., Beaudoin, N., Justes, E., 2019. Calibration and evaluation of the *STICS* soil-crop model for faba bean to explain variability in yield and N2 fixation. Eur. J. Agron. 104, 63–77. https://doi.org/10.1016/j.eja.2019.01.001.

Fall, C.M.N., Lavaysse, C., Kerdiles, H., Dramé, M.S., Roudier, P., Gaye, A.T., 2021. Performance of dry and wet spells combined with remote sensing indicators for crop yield prediction in Senegal. Clim. Risk Manag. 33, 100331. https://doi.org/10.1016/j.crm.2021.100331.

Farrell, E.J., Sherman, D.J., 2006. Process-scaling issues for aeolian transport modelling in field and wind tunnel experiments: roughness length and mass flux distributions. J. Coast. Res. 384–389.

Faye, B., Du, G., 2021. Agricultural Land transition in the "Groundnut Basin" of Senegal: 2009 to 2018. Land 10, 996. https://doi.org/10.3390/land10100996.

Freeman, P.H., 1982. Land regeneration and agricultural intensification in Senegal's groundnut basin.

Frangi, J.-P., Richards, D.C., 2000. The WELSONS experiment: overview and presentation of first results on the surface atmospheric boundary-layer in semiarid Spain. Annales Geophysicae 18, 365–384.

Fryrear, D.W., Saleh, A., 1993. Field wind erosion: vertical distribution. Soil Sci. 155, 294.

Gangneron, F., Pierre, C., Robert, É., Saqalli, M., Codiat, J., 2024. Declining field fertility in Senegal's groundnut basin: a social cohesion perspective. Mondes En Développement 205, 93–114. https://doi.org/10.3917/med.205.0093.

Garambois, N., Le Goff, U., Thibaudeau, L., 2024. Agrarian Dynamics and Climate Change in the Senegalese Sahelian Peanut Basin, in: Agrarian Systems and Climate Change, CABI Climate Change Series. pp. 15–37. DOi: 10.1079/9781800628137.0001.

Gillette, D.A., Hanson, K.J., 1989. Spatial and temporal variability of dust production caused by wind erosion in the United States. Journal of Geophysical Research: Atmospheres 94, 2197–2206. https://doi.org/10.1029/JD094iD02p02197.

Guan, K., Sultan, B., Biasutti, M., Baron, C., Lobell, D.B., 2015. What aspects of future rainfall changes matter for crop yields in West Africa? Geophys. Res. Lett. 42, 8001–8010. https://doi.org/10.1002/2015GL063877.

Guo, Z., Huang, N., Dong, Z., Van Pelt, R.S., Zobeck, T.M., 2014. Wind erosion induced soil degradation in Northern China: status, measures and perspective. Sustainability 6, 8951–8966. https://doi.org/10.3390/su6128951.

Hagen, L.J., 1991. A wind erosion prediction system to meet user needs. Journal of Soil and Water Conservation.

Havinden, M.A., 1970. The history of crop cultivation in West Africa: a bibliographical guide. Econ. Hist. Rev. 23, 532–555. https://doi.org/10.2307/2594622.

He, Y., Presley, D.R., Tatarko, J., Blanco-Canqui, H., 2018. Crop residue harvest impacts wind erodibility and simulated soil loss in the Central Great Plains. GCB Bioenergy 10, 213–226. https://doi.org/10.1111/gcbb.12483.

Hiernaux, P., Ayantunde, A., 2004. The Fakara: a semi-arid agro-ecosystem under stress. ILRI.

IUSS Working Group WRB, 2015. World Reference Base for Soil Resources. International soil classification system for naming soils and creating legends for soil maps. LCC MAKS Press. DOi: 10.29003/m4174.978-5-317-07235-3.

Jia, H., Wang, G., Guo, L., Zhuang, J., Tang, L., 2015. Wind erosion control utilizing standing corn residue in Northeast China. Soil Tillage Res. 153, 112–119. https://doi.org/10.1016/j.still.2015.05.009.
Kergoat, L., Hiernaux, P., Dardel, C., Pierre, C., Guichard, F., Kalilou, A., 2015. Dry-season vegetation mass and cover fraction from SWIR1.6 and SWIR2.1 band ratio: ground-radiometer and MODIS data in the Sahel. Int. J. Appl. Earth Obs. Geoinf. 39, 56–64. https://doi.org/10.1016/j.jag.2015.02.011.
Kidron, G.J., Karnieli, A., Benenson, I., 2009. Degradation of soil fertility following cycles of cotton–cereal cultivation in Mali, West Africa: a first approximation to the problem. Soil Tillage Res. 106, 254–262. https://doi.org/10.1016/j.still.2009.11.004.
Kok, J.F., Storelvmo, T., Karydis, V.A., Adebiyi, A.A., Mahowald, N.M., Evan, A.T., He, C., Leung, D.M., 2023. Mineral dust aerosol impacts on global climate and climate change. Nat. Rev. Earth Environ. 4, 71–86. https://doi.org/10.1038/s43017-022-00379-5.
Laurent, B., Marticorena, B., Bergametti, G., Mei, F., 2006. Modeling mineral dust emissions from Chinese and Mongolian deserts. Global and Planetary Change, Monitoring and Modelling of Asian Dust Storms 52, 121–141. DOi: 10.1016/j.gloplacha.2006.02.012.
Lebel, T., Ali, A., 2009. Recent trends in the Central and Western Sahel rainfall regime (1990–2007). Journal of Hydrology, Surface processes and water cycle in West Africa, studied from the AMMA-CATCH observing system 375, 52–64. DOi: 10.1016/j.jhydrol.2008.11.030.
Lee, J.A., Baddock, M.C., Mbuh, M.J., Gill, T.E., 2012. Geomorphic and land cover characteristics of aeolian dust sources in West Texas and eastern New Mexico, USA. Aeolian Research, The 7th International Conference on Aeolian Research (ICAR VII), Santa Rosa, Argentina 3, 459–466. DOi: 10.1016/j.aeolia.2011.08.001.
Lee, J.A., Gill, T.E., 2015. Multiple causes of wind erosion in the dust bowl. Aeolian Res. 19, 15–36. https://doi.org/10.1016/j.aeolia.2015.09.002.
Leenders, J.K., Sterk, G., Boxel, J.H., 2016. Wind erosion reduction by Scattered Woody vegetation in farmers' fields in Northern Burkina Faso. Land Degrad. Develop. 27, 1863–1872. https://doi.org/10.1002/ldr.2322.
Lericollais, A., 1970. La détérioration d'un terroir Sob, en pays Sérèr (Sénégal). Études Rurales 113–128.
Lericollais, A., Becker, C., Mbodj, M., Garenne, M., Sarr, I., Cantrelle, P., Pontié, G., Guigou, B., Garin, P., 1999. Paysans sereer: dynamiques agraires et mobilités au Sénégal, À travers champs. Éd. de l'IRD, Paris.
Leys, J., McTainsh, G., Shao, Y., 2001. Wind Erosion Monitoring and Modeling Techniques in Australia. In: Sustaining the Global Farm. Presented at the 10th International Soil Conservation Organization Meeting. Purdue University, USDA-ARS National Soil Erosion Research Laboratory.
Li, J., Okin, G.S., Alvarez, L., Epstein, H., 2007. Quantitative effects of vegetation cover on wind erosion and soil nutrient loss in a desert grassland of southern New Mexico, USA. Biogeochemistry 85, 317–332. https://doi.org/10.1007/s10533-007-9142-y.
Lyles, L., 1975. Possible effects of wind erosion on soil productivity. J. Soil Water Conserv. 30, 279–283.
Mainguet, M., Chemin, M.C., 1991. Wind degradation on the sandy soils of the Sahel of Mali and Niger and its part in desertification, in: Barndorff-Nielsen, O.E., Willetts, B. B. (Eds.), Aeolian Grain Transport. Springer, Vienna, pp. 113–130. DOi: 10.1007/978-3-7091-6703-8_9.
Malou, O.P., Moulin, P., Chevallier, T., Masse, D., Vayssières, J., Badiane-Ndour, N.Y., Tall, L., Thiam, A., Chapuis-Lardy, L., 2021. Estimates of carbon stocks in sandy soils cultivated under local management practices in Senegal's groundnut basin. Reg. Environ. Chang. 21, 65. https://doi.org/10.1007/s10113-021-01790-2.
Marsham, J.H., Knippertz, P., Dixon, N.S., Parker, D.J., Lister, G.M.S., 2011. The importance of the representation of deep convection for modeled dust-generating winds over West Africa during summer: summertime dust uplift over west Africa. Geophys. Res. Lett. 38, n/a-n/a. https://doi.org/10.1029/2011GL048368.
Marticorena, B., Bergametti, G., 1995. Modeling the athmospheric dust cycle : 1. Design of a soil-derived dust emission scheme. J. Geophys. Res. 100, 16415–16430. https://doi.org/10.1029/95JD00690.
Marticorena, B., Kardous, M., Bergametti, G., Callot, Y., Chazette, P., Khatteli, H., Le Hégarat-Mascle, S., Maillé, M., Rajot, J.-L., Vidal-Madjar, D., Zribi, M., 2006. Surface and aerodynamic roughness in arid and semiarid areas and their relation to radar backscatter coefficient: surface roughness in Arid areas. J. Geophys. Res. 111. https://doi.org/10.1029/2006JF000462.
[dataset] Marticorena, B., Dorego, G.S., Rajot, J.L., Bouet, C., Allègre, M., Chatenet, B., Féron, A., Gaimoz, C., Maisonneuve, F., Siour, G., Valorso, R., Diop, M., Der Ba, S., Rokhy N'Diaye, G., Séné, M. & Thiam, A. (2021). Wind speed, Air temperature, Precipitation amount, Relative Humidity, Bambey, Senegal.. Aeris. DOi: 10.25326/270, DOi: 10.25326/263, DOi: 10.25326/266, DOi: 10.25326/265.
Masse, D., Lalou, R., Tine, C., Ba, M., Vayssières, J., 2018. Chapitre 16. Les trajectoires agricoles dans le Bassin Arachidier au Sénégal : éléments de réflexion à partir de l'observatoire de Niakhar, in: Delaunay, V., Desclaux, A., Sokhna, C. (Eds.), Niakhar, mémoires et perspectives. IRD Éditions, pp. 311–332. DOi: 10.4000/books.irdeditions.31687.
Mctainsh, G.H., Lynch, A.W., Burgess, R.C., 1990. Wind erosion in eastern Australia. Soil Res. 28, 323–339. https://doi.org/10.1071/sr9900323.
Mendez, M.J., Buschiazzo, D.E., 2015. Soil coverage evolution and wind erosion risk on summer crops under contrasting tillage systems. Aeolian Res. 16, 117–124. https://doi.org/10.1016/j.aeolia.2014.12.002.
Middleton, N.J., 2017. Desert dust hazards: a global review. Aeolian Res. 24, 53–63. https://doi.org/10.1016/j.aeolia.2016.12.001.
Monin, A.S., Obukhov, A.M., 1954. Basic laws of turbulent mixing in the surface layer of the atmosphere. Main Geophysical Observatory and the Geophysical Institute of the Academy of Sciences of the USSR 24, 163–187.
Mougin, E., Diawara, M.O., Soumaguel, N., Maïga, A.A., Demarez, V., Hiernaux, P., Grippa, M., Chaffard, V., Ba, A., 2019. A leaf area index data set acquired in Sahelian rangelands of Gourma in Mali over the 2005–2017 period. Earth Syst. Sci. Data 11, 675–686. https://doi.org/10.5194/essd-11-675-2019.
Mougin, E., Lo Seena, D., Rambal, S., Gaston, A., Hiernaux, P., 1995. A regional Sahelian grassland model to be coupled with multispectral satellite data. I: Model description and validation. Remote Sens. Environ. 52, 181–193. https://doi.org/10.1016/0034-4257(94)00126-8.
Naab, J.B., Singh, P., Boote, K.J., Jones, J.W., Marfo, K.O., 2004. Using the CROPGRO-peanut model to quantify yield gaps of peanut in the Guinean Savanna Zone of Ghana. Agron. J. 96, 1231–1242. https://doi.org/10.2134/agronj2004.1231.
Nandintsetseg, B., Shinoda, M., 2015. Land surface memory effects on dust emission in a Mongolian temperate grassland. Journal of Geophysical Research: Biogeosciences 120, 414–427. https://doi.org/10.1002/2014JG002708.
Nordstrom, K.F., Hotta, S., 2004. Wind erosion from cropland in the USA: a review of problems, solutions and prospects. Geoderma 121, 157–167. https://doi.org/10.1016/j.geoderma.2003.11.012.
Nzabarinda, V., Bao, A., Xu, W., Uwamahoro, S., Huang, X., Gao, Z., Umugwaneza, A., Kayumba, P.M., Maniraho, A.P., Jiang, Z., 2021. Impact of cropland development intensity and expansion on natural vegetation in different African countries. Eco. Inform. 64, 101359. https://doi.org/10.1016/j.ecoinf.2021.101359.
OECD, Sahel and West Africa Club, 2014. An Atlas of the Sahara-Sahel: Geography, Economics and Security, West African Studies. OECD. DOi: 10.1787/9789264222359-en.
Osborne, S.L., Johnson, J.M.F., Jin, V.L., Hammerbeck, A.L., Varvel, G.E., Schumacher, T.E., 2014. The Impact of corn residue removal on soil aggregates and particulate organic matter. Bioenerg. Res. 7, 559–567. https://doi.org/10.1007/s12155-014-9413-0.
Pélissier, P., 1966. Les Paysans du Sénégal: les civilisations agraires du Cayor à la Casamance Impr. Fabrègue.
Pierre, C., Bergametti, G., Marticorena, B., AbdourhamaneTouré, A., Rajot, J.-L., Kergoat, L., 2014a. Modeling wind erosion flux and its seasonality from a cultivated Sahelian surface: a case study in Niger. Catena 122, 61–71. https://doi.org/10.1016/j.catena.2014.06.006.
Pierre, C., Bergametti, G., Marticorena, B., Kergoat, L., Mougin, E., Hiernaux, P., 2014b. Comparing drag partition schemes over a herbaceous Sahelian rangeland. J. Geophys. Res. Earth 119, 2291–2313. https://doi.org/10.1002/2014JF003177.
Pierre, C., Grippa, M., Mougin, E., Guichard, F., Kergoat, L., 2016. Changes in Sahelian annual vegetation growth and phenology since 1960: a modeling approach. Global Planet. Change 143, 162–174. https://doi.org/10.1016/j.gloplacha.2016.06.009.
Pierre, C., Kergoat, L., Bergametti, G., Mougin, É., Baron, C., Abdourhamane Toure, A., Rajot, J.-L., Hiernaux, P., Marticorena, B., Delon, C., 2015. Modeling vegetation and wind erosion from a millet field and from a rangeland: two Sahelian case studies. Aeolian Res. 19, 97–111. https://doi.org/10.1016/j.aeolia.2015.09.009.
Pierre, C., Kergoat, L., Hiernaux, P., Baron, C., Bergametti, G., Rajot, J.-L., Abdourhamane Toure, A., Okin, G.S., Marticorena, B., 2018. Impact of agropastoral management on wind erosion in Sahelian croplands: agropastoral management impact on wind erosion in Sahelian croplands. Land Degrad. Develop. 29, 800–811. https://doi.org/10.1002/ldr.2783.
Pierre, C., Rajot, J.L., Faye, I., Dorego, G.S., Bouet, C., Marticorena, B., Bergametti, G., Ka, A., Amar, B., Tall, A., Diagne, N., Feron, A., 2023. A contrasting seasonality of wind erosivity and wind erosion between Central and Western Sahel. Aeolian Res. 62, 100879. https://doi.org/10.1016/j.aeolia.2023.100879.
Pires, M., 2012. A historical political ecology of land use in the southeastern peanut basin of Senegal. Afr. Geogr. Rev. 31, 95–110. https://doi.org/10.1080/19376812.2012.715992.
Priestley, C.H.B., 1959. Turbulent transfer in the lower atmosphere. Q. J. R. Meteorolog. Soc. 86, 290. https://doi.org/10.1002/qj.49708636825.
Rajot, J.-L., 2001. Wind blown sediment mass budget of Sahelian village land units in Niger. Bulletin De La Société Géologique De France 172, 523–531. https://doi.org/10.2113/172.5.523.
Rajot, J.L., Alfaro, S.C., Gomes, L., Gaudichet, A., 2003. Soil crusting on sandy soils and its influence on wind erosion. Catena 53, 1–16. https://doi.org/10.1016/S0341-8162(02)00201-1.
Ranaivoson, L., Falconnier, G.N., Affholder, F., Leroux, L., Autfray, P., Muller, B., Auzoux, S., Ripoche, A., 2022. Can green manure contribute to sustainable intensification of rainfed rice production in Madagascar? Field Crop Res 289, 108711. https://doi.org/10.1016/j.fcr.2022.108711.
Ricome, A., Affholder, F., Gérard, F., Muller, B., Poeydebat, C., Quirion, P., Sall, M., 2017. Are subsidies to weather-index insurance the best use of public funds? a bio-economic farm model applied to the Senegalese groundnut basin. Agr. Syst. 156, 149–176. https://doi.org/10.1016/j.agsy.2017.05.015.
Sambou, A., Seye, M., Foncéka, D., 2022. Assessment of Farmers' Groundnut Varietal Trait Preferences and Production Constraints in the Groundnut Basin of Senegal.
Santra, P., Moharana, P.C., Kumar, M., Soni, M.L., Pandey, C.B., Chaudhari, S.K., Sikka, A.K., 2017. Crop production and economic loss due to wind erosion in hot arid ecosystem of India. Aeolian Res. 28, 71–82. https://doi.org/10.1016/j.aeolia.2017.07.009.
Schlecht, E., Hiernaux, P., 2001. Mobilité régionale du bétail: nécessité et alternatives?.
Skidmore, E., Kumar, M., Larson, W.E., 1979. Crop residue management for wind erosion control in the Great Plains.
Sow, S., Senghor, Y., Sadio, K., Vezy, R., Roupsard, O., Affholder, F., N'dienor, M., Clermont-Dauphin, C., Gaglo, E.K., Ba, S., Tounkara, A., Balde, A.B., Agbohessou, Y., Seghieri, J., Sall, S.N., Couedel, A., Leroux, L., Jourdan, C., Diaite, D.S., Falconnier, G.N., 2024. Calibrating the STICS soil-crop model to explore the impact of

agroforestry parklands on millet growth. Field Crops Research 306, 109206. DOi: 10.1016/j.fcr.2023.109206.
Sivakumar, M.V.K., 1988. Predicting rainy season potential from the onset of rains in Southern Sahelian and Sudanian climatic zones of West Africa. Agricultural and Forest Meteorology 42, 295–305. https://doi.org/10.1016/0168-1923(88)90039-1.
Spaan, W.P., van den Abeele, G.D., 1991. Wind borne particle measurements with acoustic sensors. Soil Technol. 4, 51–63. https://doi.org/10.1016/0933-3630(91)90039-P.
Sterk, G., 2003. Causes, consequences and control of wind erosion in Sahelian Africa: a review. Land Degrad. Dev. 14, 95–108. https://doi.org/10.1002/ldr.526.
Sterk, G., Herrmann, L., Bationo, A., 1996. Wind-blown nutrient transport and soil productivity changes in southwest Niger. Land Degrad. Dev. 7, 325–335. https://doi.org/10.1002/(SICI)1099-145X(199612)7:4<325::AID-LDR237>3.0.CO;2-Q.
Sterk, G., Raats, P.A.C., 1996. Comparison of models describing the vertical distribution of wind-eroded sediment. Soil Sci. Soc. Am. J. 60, 1914–1919. https://doi.org/10.2136/sssaj1996.03615995006000060042x.
Sterk, G., Riksen, M., Goosen, D.i., 2001. Dryland degradation by wind erosion and its control. Ann. Arid Zone 40, 351–367.
Sterk, G., Spaan, W.P., 1997. Wind erosion control with crop residues in the Sahel. Soil Sci. Soc. Am. J. 61, 911–917. https://doi.org/10.2136/sssaj1997.03615995006100030028x.
Tappan, G.G., Cushing, W.M., Cotillon, S.E., Hutchinson, J.A., Pengra, B., Alfari, I., Botoni, E., Soulé, A., Herrmann, S.M., 2016. Landscapes of West Africa: A window on a changing world. DOi: 10.5066/F7N014QZ.
Tracol, Y., Mougin, E., Hiernaux, P., Jarlan, L., 2006. Testing a sahelian grassland functioning model against herbage mass measurements. Ecol. Model. 193, 437–446. https://doi.org/10.1016/j.ecolmodel.2005.08.033.
Traoré, A., Falconnier, G.N., Ba, A., Sissoko, F., Sultan, B., Affholder, F., 2022. Modeling sorghum-cowpea intercropping for a site in the savannah zone of Mali: strengths and weaknesses of the stics model. Field Crop Res 285, 108581. https://doi.org/10.1016/j.fcr.2022.108581.
Tschakert, P., 2004. Carbon for farmers: assessing the potential for soil carbon sequestration in the old peanut basin of Senegal. Clim. Change 67, 273–290. https://doi.org/10.1007/s10584-004-1821-2.
Tschakert, P., Tappan, G., 2004. The social context of carbon sequestration: considerations from a multi-scale environmental history of the old peanut basin of Senegal. J. Arid Environ. 59, 535–564. https://doi.org/10.1016/j.jaridenv.2004.03.021.
Turner, M.D., Hiernaux, P., 2002. The use of herders' accounts to map livestock activities across agropastoral landscapes in Semi-Arid Africa. Landsc. Ecol. 17, 367–385. https://doi.org/10.1023/A:1021238208019.
Visser, S.M., Sterk, G., 2007. Nutrient dynamics—wind and water erosion at the village scale in the Sahel. Land Degrad. Dev. 18, 578–588. https://doi.org/10.1002/ldr.800.
Visser, S.M., Sterk, G., Karssenberg, D., 2005. Wind erosion modelling in a Sahelian environment. Environ. Model. Software 20, 69–84. https://doi.org/10.1016/j.envsoft.2003.12.010.
Vos, H.C., Karst, I.G., Eckardt, F.D., Fister, W., Kuhn, N.J., 2022. Influence of Crop and land management on wind erosion from sandy soils in dryland agriculture. Agronomy 12, 457. https://doi.org/10.3390/agronomy12020457.
Wang, E., Harman, W.L., Williams, J.R., Xu, C., 2002. Simulated effects of crop rotations and residue management on wind erosion in Wuchuan, West-Central Inner Mongolia, China. J. Environ. Qual. 31, 1240–1247. https://doi.org/10.2134/jeq2002.1240.
Webb, N.P., Van Zee, J.W., Karl, J.W., Herrick, J.E., Courtright, E.M., Billings, B.J., Boyd, R., Chappell, A., Duniway, M.C., Derner, J.D., Hand, J.L., Kachergis, E., McCord, S.E., Newingham, B.A., Pierson, F.B., Steiner, J.L., Tatarko, J., Tedela, N.H., Toledo, D., Scott Van Pelt, R., 2017. Enhancing Wind Erosion Monitoring and Assessment for U.S. Rangelands. Rangelands 39, 85–96. https://doi.org/10.1016/j.rala.2017.04.001.
Wiggs, G., Holmes, P., 2011. Dynamic controls on wind erosion and dust generation on west-central free state agricultural land, South Africa. Earth Surf. Proc. Land. 36, 827–838. https://doi.org/10.1002/esp.2110.
Woodruff, N.P., Siddoway, F.H., 1965. A Wind erosion equation. Soil Sci. Soc. Am. J. 29, 602–608. https://doi.org/10.2136/sssaj1965.03615995002900050035x.
Zabel, F., Delzeit, R., Schneider, J.M., Seppelt, R., Mauser, W., Václavík, T., 2019. Global impacts of future cropland expansion and intensification on agricultural markets and biodiversity. Nat. Commun. 10, 2844. https://doi.org/10.1038/s41467-019-10775-z.
Zhang, W., Brandt, M., Tong, X., Tian, Q., Fensholt, R., 2018. Impacts of the seasonal distribution of rainfall on vegetation productivity across the Sahel. Biogeosciences 15, 319–330. https://doi.org/10.5194/bg-15-319-2018.
Zobeck, T.M., 1991. Abrasion of crusted soils: influence of abrader flux and soil properties. Soil Sci. Soc. Am. J. 55, 1091–1097. https://doi.org/10.2136/sssaj1991.03615995005500040033x.